Advanced Computational Study of Nonlinear Time-Fractional Newell-Whitehead-Segel Equation with Caputo-Fabrizio Derivative Using B-Spline Techniques

Marryam Shafique[1,2], Muhammad Yaseeen[1,*], Salma Trabelsi[3] and Marwa Balti[3,*]

[1] Department of Mathematics, University of Sargodha, Sargodha, Pakistan

[2] Department of Mathematics, Baba Guru Nanak University, Adampura, Nankana Sahib, Pakistan

[3] Department of Mathematics and Statistics, College of Science, King Faisal University, Al Ahsa, Saudi Arabia

INFORMATION

Keywords:
Trigonometric
cubic and extended cubic
B-splines
time fractional differential
equations
Caputo-Fabrizo fractional
derivative
Newell-Whitehead-Segel equation
stability
convergence

DOI: 10.23967/j.rimni.2026.10.72284

SCIPEDIA Revista Internacional de Métodos Numéricos para Cálculo y Diseño en Ingeniería

Revista Internacional Métodos numéricos para cálculo y diseño en ingeniería RIMNI

In cooperation with CIMNE

Advanced Computational Study of Nonlinear Time-Fractional Newell-Whitehead-Segel Equation with Caputo-Fabrizio Derivative Using B-Spline Techniques

Marryam Shafique[1,2], **Muhammad Yaseeen**[1,*], **Salma Trabelsi**[3] **and Marwa Balti**[3,*]

[1]Department of Mathematics, University of Sargodha, Sargodha, Pakistan

[2]Department of Mathematics, Baba Guru Nanak University, Adampura, Nankana Sahib, Pakistan

[3]Department of Mathematics and Statistics, College of Science, King Faisal University, Al Ahsa, Saudi Arabia

ABSTRACT

This study presents numerical solutions for the time-fractional Newell-Whitehead-Segel (NWS) equation with a Caputo-Fabrizio derivative. Spatial derivatives are discretized using three B-splines-cubic, cubic trigonometric and extended cubic B-splines-while temporal discretization is handled by a finite difference scheme. The proposed schemes are rigorously analyzed for stability and convergence. Their performance is evaluated in terms of accuracy and computational efficiency. Numerical experiments confirm the effectiveness of these techniques in capturing the dynamics of the fractional NWS equation. Each B-spline variant demonstrates unique strengths, highlighting the flexibility of B-spline approaches for solving fractional differential equations with nonlocal, memory-dependent operators. These results affirm the reliability and robustness of B-spline-based methods for such problems, paving the way for future advancements in this area.

OPEN ACCESS

Received: 23/08/2025

Accepted: 08/12/2025

Published: 16/04/2026

DOI
10.23967/j.rimni.2026.10.72284

Keywords:
Trigonometric
cubic and extended cubic B-splines
time fractional differential equations
Caputo-Fabrizo fractional derivative
Newell-Whitehead-Segel equation
stability
convergence

1 Introduction

The time-fractional Newell-Whitehead-Segel (NWS) equation [1] is given by:

$$\frac{\partial^\gamma v(s,t)}{\partial t^\gamma} = k\frac{\partial^2 v(s,t)}{\partial s^2} + av(s,t) - b(v(s,t))^q, 0 < \gamma \leq 1, s \in \Omega = [0,1], t \geq 0, \tag{1}$$

subject to the initial condition

$$v(s,t) = f(s), \quad t = 0,$$

*Correspondence: Muhammad Yaseeen, Marwa Balti (yaseen.yaqoob@uos.edu.pk, mbalti@kfu.edu.sa).

and boundary condition

$$u(0,t) = \phi_1(t) \quad \text{and} \quad u(1,t) = \phi_2(t) \quad t > 0,$$

where a, b, k are real parameters with $k > 0$, q is a positive integer and $\phi_1(t), \phi_2(t), f(s)$ are known functions. The time-fractional NWS equation finds important applications across multiple disciplines, including pattern formation in biological systems, chemical reaction-diffusion processes, neural dynamics, ecological population modeling and Rayleigh-Bénard convection in fluid dynamics. The fractional order γ introduces crucial memory effects that capture anomalous diffusion and hereditary properties observed in these complex systems, providing more realistic modeling of subdiffusive transport and long-range spatial interactions than classical integer-order approaches.

The fractional derivative in (1) is defined in the Caputo-Fabrizio sense as:

$${}_0^{CF}\mathfrak{D}_t^{\gamma} v(s,t) = \frac{M(\gamma)}{1-\gamma} \int_0^t \frac{\partial v(s,t)}{\partial y} exp\left[-\gamma \frac{t-y}{1-\gamma}\right] dy,$$

where $v'(s,y) \in H^1(s,y), b > 0$ and $M(\gamma)$ is the normalization constant that satisfies $M(0) = M(1) = 1$.

Fractional differential equations (FDEs) have gained significant attention due to their ability to describe complex systems with non-local and memory-dependent dynamics such as anomalous diffusion and heriditary processes. Applications span a wide range of fields, including tumor growth [2], random walks [3], continuum mechanics [4], viscoplastic and viscoelastic flows [5], control theory [6], transport phenomena [7] and turbulence [8,9].

Due to the lack of closed-form solutions for most FDEs, numerical methods play a central role in their study.

The time-fractional NWS equation represents an important extension of the classical NWS model, incorporating fractional derivatives to capture memory-dependent dynamics and anomalous diffusion processes. The Caputo-Fabrizio fractional derivative operator is employed in this study due to its specific physical and mathematical advantages for modeling the NWS equation. Unlike singular kernel operators, the CF derivative features a non-singular exponential kernel that more realistically represents certain physical processes, particularly those exhibiting exponential decay of memory effects. This formulation is especially suitable for modeling pattern formation phenomena where the memory effect diminishes exponentially over time, as observed in various reaction-diffusion systems. The CF operator has been successfully applied in numerous physical contexts including viscoelastic materials, thermal systems with fading memory, and biological processes with exponential relaxation behavior. For the NWS equation specifically, the CF derivative captures the gradual, exponentially decaying memory effects that characterize the evolution of amplitude modulations in convective instabilities and biological pattern formation. Recent studies have employed various analytical and numerical approaches to investigate this equation.

Korkmaz [10] explored complex wave solutions for the NWS equation using advanced methods to uncover complicated behaviors. Kumar and Sharma [11] investigated the NWS equation of fractional order to develop its numerical approximation. Patel et al. [12] developed the technique for finding exact solutions to the NWS equation using the semi-analytical approach. Kumar and Yadav [13] applied deep learning method to solve the NWS equation. Bekela and Deresse [14] presented an efficient numerical technique for solving nonlinear fractional hyperbolic partial differential equations usig fractional Shehu transform iterative method. Shawagfeh [15] explored analytical approximate solutions for NWS equation. Patade and Bhalekar [16] introduced a novel iterative approach to obtain approximate

analytical solutions of the NWS equation. Saadeh et al. [17] applied a fractional residual power series algorithm to address the NWS equation in fractional order. Luo and Nadeem [18] extended the solution space of the time-fractional NWS model by employing the Laplace residual power series method. Saravanan and Magesh [19] conducted a comparative analysis between the reduced differential transform method and the Adomian decomposition method for the NWS equation. Ayata and Ozkan [20] proposed a conformable Laplace decomposition method to solve the fractional NWS equation. Prakash et al. [21] utilized the fractional variational iteration method to solve the time-fractional NWS equation employing the Caputo derivative operator, while Areshi et al. [22] investigated the fractional-order Newell–Whitehead–Segel equation using the Atangana–Baleanu fractional derivative. In contrast, our work employs the Caputo-Fabrizio fractional derivative, which offers distinct mathematical properties including a non-singular kernel. The application of the Caputo-Fabrizio operator to the NWS equation represents a novel aspect of our study. Exact and approximate solutions are compared through graphs and tables, showing excellent agreement and high accuracy. Jassim [23] applied the Homotopy Perturbation Transform Method (HPTM) to solve the Newell–Whitehead–Segel equation. By combining the Laplace transform with the homotopy perturbation technique, an efficient series solution was obtained. Newell and Whitehea [24] presented a theoretical study on finite-bandwidth, finite-amplitude convection in fluid systems. They derived the Newell–Whitehead–Segel (NWS) equation to describe pattern formation near the onset of convection. The work established a fundamental model in nonlinear fluid dynamics, explaining how amplitude modulations evolve in convective instabilities. They derived the Newell–Whitehead–Segel (NWS) equation to describe pattern formation near the onset of convection. The work established a fundamental model in nonlinear fluid dynamics, explaining how amplitude modulations evolve in convective instabilities. Jani and Singh [25] express the solution as an infinite series via HPM, transform differential operators using the Aboodh transform, and derive recurrence relations for the series coefficients. They also analyze convergence and provide numerical examples demonstrating good agreement with exact or known solutions. Caputo and Fabrizio [26,27] introduced a new fractional derivative with an exponential (non-singular) kernel. This derivative, known as the Caputo–Fabrizio derivative, eliminates the singularity present in classical fractional operators. It provides a smooth, physically meaningful model for processes with memory effects, suitable for Laplace. Venkateswaran et al. [28] present a hybrid simulation framework (combining discrete-event and continuous simulation) to model and plan in a Vendor Managed Inventory (VMI) supply chain. Their method captures both operational dynamics (e.g., replenishment, inventory flow) and planning decisions (e.g., shipment scheduling, vendor vs. retailer control). Yousif and Hamasalh [29] discuss a hybrid numerical method that couples non-polynomial spline interpolation with a conformable fractional continuity equation (CCE) to solve nonlinear time-fractional differential equations. They prove stability (via Fourier method) and analyze convergence order, showing the scheme works robustly under certain parameter ranges. Previous research has explored various solution methods, but B-spline methods have never been used for the fractional NWS equation. This body of work has significantly advanced our understanding of the solution space and the behavior of the fractional NWS equation. The main contributions of this study are:

- A novel B-spline-based numerical framework is developed for solving the nonlinear time-fractional NWS equation involving the Caputo-Fabrizio derivative.
- Three types of B-spline basis functions–cubic, trigonometric cubic, and extended cubic—are employed for spatial discretization, enabling a comparative performance analysis.
- A finite difference method is used for temporal discretization and the combined scheme is analyzed for stability and convergence.

- Comprehensive numerical experiments are conducted to validate the proposed methods and demonstrate their accuracy and efficiency.

The remainder of this paper is structured as follows. Section 2 describes the proposed numerical scheme and its mathematical formulation. Section 3 provides a rigorous stability analysis of the method. Section 4 discusses the convergence properties. Section 5 presents and analyzes the numerical results. Section 6 presents physical interpretation of the numerical results. Finally, Section 7 concludes the paper with a summary and suggestions for future work.

2 Numerical Schemes

This section develops numerical techniques using three classes of B-Spline functions–cubic, extended cubic and trigonometric cubic B-Splines for solving the time-fractional NWS (Eq. (1)).

Let $\tau = \dfrac{T}{N}$ and $h = \dfrac{L}{M}$ denote temporal and spatial step sizes, respectively, where $M, N \in \mathbb{Z}^+$. We define:

- Temporal nodes: $t_m = m\tau$ for $m = 0, 1, \cdots, N$
- Spatial nodes: $s_j = jh$ for $j = 0, 1, \cdots, M$
- Solution domain: $\Delta = [a, b]$ partioned into M equal subintervals $[s_j, s_{j+1}]$

2.1 Trigonometric Cubic B-Spline Scheme

The approximate solution $V(s, t)$ is constructed as:

$$V(s,t) = \sum_{j=-1}^{M+1} C_j(t)\, TB_j^4(s), \tag{2}$$

where $C_j(t)$ are time-dependent coefficients and $TB_j^4(s)$ are trigonometric cubic B-Splines (TCuBS) basis functions [30]:

$$TB_j^4(s) = \frac{1}{p}\begin{cases} l^3(s_j), & s \in [s_j, s_{j+1}) \\ l(s_j)(l(s_j)m(s_{j+2}) + m(s_{j+3})l(s_{j+1})) + m(s_{j+4})l^2(s_{j+1}), & s \in [s_{j+1}, s_{j+2}) \\ m(s_{j+4})(l(s_{j+1})m(s_{j+3}) + m(s_{j+4})l(s_{j+2})) + l(s_j)m^2(s_{j+3}), & s \in [s_{j+2}, s_{j+3}) \\ m^3(s_{j+4}), & s \in [s_{j+3}, s_{j+4}), \end{cases} \tag{3}$$

with $l(s_j) = \sin\left(\dfrac{s - s_j}{2}\right), m(s_j) = \sin\left(\dfrac{s_j - s}{2}\right)$ and $p = \sin\left(\dfrac{h}{2}\right)\sin(h)\sin\left(\dfrac{3h}{2}\right)$.

The set $\{T_{-3,4}, T_{-2,4}, \ldots, T_{M-2,4}, T_{M-1,4}\}$ forms a basis over $[a, b]$. Due to the local support property of trignometric B-splines, only three non-zero basis functions $T_{j-3,4}(s)$, $T_{j-2,4}(s)$ and $T_{j-1,4}(s)$ contribute at the grid point (s_j, t^M). Thus the approximate solution at the M-th time level is given by:

$$v_j^m = \sum_{w=j-1}^{j+1} C_w^m(t)\, TB_w^4(s) \tag{4}$$

where C_j^m are time-dependent unknowns calculated using initial and boundary conditions. The differential equation is enforced at the spatial nodes $s_j = jh$ for $j = 0, 1, \ldots, M$, which serve as our collocation points. At these collocation points, the approximate solutions and their derivatives are

expressed in terms of C_j^m as:

$$\begin{cases} v_j^m = a_1 C_{j-1}^m + a_2 C_j^m + a_1 C_{j+1}^m, \\ (v_j^m)_s = -b_1 C_{j-1}^m + b_2 C_{j+1}^m + b_3 C_{j+1}^m, \\ (v_j^m)_{ss} = c_1 C_{j-1}^m + c_2 C_j^m + c_1 C_{j+1}^m, \end{cases} \tag{5}$$

where coefficients a_i, b_i, c_i are given in (6).

$$\begin{cases} a_1 = \csc(h)\csc\left(\frac{3h}{2}\right)\sin^2\left(\frac{h}{2}\right), \\ a_2 = \frac{2}{1+2\cos(h)}, \\ b_1 = \frac{3}{4}\csc\left(\frac{3h}{2}\right), \\ b_2 = 0, \\ c_1 = \frac{3+9\cos(h)}{4\cos\left(\frac{h}{2}\right)} - 4\cos\left(\frac{5h}{2}\right), \\ c_2 = -\frac{3\cot^2\left(\frac{h}{2}\right)}{2+4\cos(h)}. \end{cases} \tag{6}$$

The Caputo-Fabrizio derivative is approximated as [31]:

$${}_0^{CF}\mathfrak{D}_t^{\gamma} v(s_j, t_{m+1}) = \begin{cases} w_0[M_{k+1}^{k+1}(v^{k+1}(x) - v^k(x)) + \sum_{j=1}^{k}(v^j(x) - v^{j-1}(x))M_j^{k+1}], & k \geq 1, \\ w_0 M_1^1(v^1(x) - v^0(x)), & k = 0, \end{cases} \tag{7}$$

where $w_0 = (\gamma\tau)^{-1}$ and M_j^k defined in (8) satisfies the properties of Lemmas 1–2.

$$M_j^k = \exp(-\gamma\tau\frac{k+1-j}{1-\gamma}) - \exp(-\gamma\tau\frac{k-j+2}{1-\gamma})), \quad j = 1, 2, \ldots k-1. \tag{8}$$

Lemma 1: *[32] From the definition in (8), we have:*

$M_j^k > 0, \quad M_{j+1}^k = M_j^{k-1}, \quad M_{j+1}^k = M_j^{k-1}$ and $M_j^k \leq M_{j+1}^k \quad \forall j \leq k.$

Lemma 2: *[33] Let $v(t) \in C_{s,t}^{4,4}([0, L] \times [0, T])$. Then:*

$0 \leq M_j - M_{j+1} \leq C\tau M_j$ *and* $0 \leq M_j \leq C\tau,$

where C Positive constant independent of j.

The discretized form of (1) is:

$${}_0^{CF}\mathfrak{D}_t^{\gamma} v(s_j, t_{n+1}) = k(v_j^{n+1})_{ss} + a(v_j^{n+1}) - b(v_j^n)^q, \quad 0 < \gamma \leq 1. \tag{9}$$

For $n = 0$, we have:

$$w_0 M_1^1 (v^1(x) - v^0) = k(v_j^1)_{ss} + a(v_j^1) - b(v_j^0)^q. \tag{10}$$

Using the TCuBS approximations (5) into (21), we get:

$$\eta_1 C_{j-1}^1 + \eta_2 C_j^1 + \eta_1 C_{j+1}^1 = w_0 M_1^1 \left(a_1 C_{j-1}^0 + a_2 C_j^0 + a_1 C_{j+1}^0\right) - b\left(a_1 C_{j-1}^0 + a_2 C_j^0 + a_1 C_{j+1}^0\right)^q,$$

where $\eta_1 = w_0 M_1^1 a_1 - kc_1 - aa_1$ and $\eta_2 = w_0 M_1^1 a_2 - kc_2 - aa_2$. In matrix form:

$$A_3 C^1 = w_0 M_1^1 A_2 C^0 - b(A_2 C^0)^q,$$

where:

$$A_2 = \begin{bmatrix} a_1 & a_2 & a_1 & 0 & \dots & 0 \\ 0 & a_1 & a_2 & a_1 & \ddots & \vdots \\ \vdots & \ddots & \ddots & \ddots & \ddots & 0 \\ 0 & \dots & a_1 & a_2 & a_1 & 0 \\ 0 & \dots & 0 & a_1 & a_2 & a_1 \end{bmatrix}, \quad A_3 = \begin{bmatrix} \eta_1 & \eta_2 & \eta_1 & 0 & \dots & 0 \\ 0 & \eta_1 & \eta_2 & \eta_1 & \ddots & \vdots \\ \vdots & \ddots & \ddots & \ddots & \ddots & 0 \\ 0 & \dots & \eta_1 & \eta_2 & \eta_1 & 0 \\ 0 & \dots & 0 & \eta_1 & \eta_2 & \eta_1 \end{bmatrix}.$$

For $n \geq 1$, the scheme becomes:

$$w_0[M_{n+1}^{n+1}(v^{n+1}(x) - v^n + \sum_{j=1}^{n}(v^j(x) - v^{J-1}(x))M_j^{n+1}] = k(v_j^{n+1})_{ss} + a(v_j^{n+1}) - b(v_j^n)^q. \tag{11}$$

Using the TCuBS approximations (5) in above equation, we obtain:

$$\begin{aligned} \eta_3 C_{j-1}^{n+1} + \eta_4 C_j^{n+1} + \eta_3 C_{j+1}^{n+1} = {} & w_0 M_{n+1}^{n+1} \left(a_1 C_{j-1}^n + a_2 C_j^n + a_1 C_{j+1}^n\right) \\ & - \sum_{j=1}^{n} M_j^{n+1} \Big[(a_1 C_{j-1}^j + a_2 C_j^j + a_1 C_{j+1}^j) \\ & - (a_1 C_{j-1}^{j-1} + a_2 C_j^{j-1} + a_1 C_{j+1}^{j-1}) \Big] \\ & - b\left(a_1 C_{j-1}^n + a_2 C_j^n + a_1 C_{j+1}^n\right)^q, \end{aligned} \tag{12}$$

where $\eta_3 = w_0 M_{n+1}^{n+1} a_1 - kc_1 - aa_1$ and $\eta_4 = w_0 M_{n+1}^{n+1} a_2 - kc_2 - aa_2$.

In matrix form:

$$A_4 C^{n+1} = w_0 M_{n+1}^{n+1} A_2 C^n - b(A_2 C^n)^q - \sum_{j=1}^{n}(C^j - C^{j-1}) M_j^{n+1},$$

where

$$A_4 = \begin{bmatrix} \eta_3 & \eta_4 & \eta_3 & 0 & \dots & 0 \\ 0 & \eta_3 & \eta_4 & \eta_3 & \ddots & \vdots \\ \vdots & \ddots & \ddots & \ddots & \ddots & 0 \\ 0 & \dots \eta_3 & \eta_4 & \eta_3 & 0 & \\ 0 & \dots & 0 & \eta_3 & \eta_4 & \eta_3 \end{bmatrix}.$$

The above system consists of $(M+1)$ equations in $(M+3)$ unknowns. To ensure a unique solution, two additional equations are needed. We use the boundary conditions for this purpose as follows:

$$v_0^{n+1} = \zeta_1 C_{-1}^{m+1} + \zeta_2 C_0^{m+1} + \zeta_1 C_1^{m+1} = \phi_1(t^{n+1}), \tag{13}$$

$$v_M^{n+1} = \zeta_1 C_{M-1}^{m+1} + \zeta_2 C_M^{m+1} + \zeta_1 C_{M+1}^{m+1} = \phi_2(t^{n+1}). \tag{14}$$

The complete system for each time level $n+1$ then consists of:

- $M+1$ equations from the collocation at interior spatial points,
- 2 equations from the boundary (Eqs. (13) and (14)).

Eqs. (12)–(14) yield a nonlinear system of $M+3$ equations in $M+3$ unknowns $C_{-1}^{n+1}, C_0^{n+1}, \ldots, C_{M+1}^{n+1}$, which can be efficiently solved using a suitable numerical solver.

2.2 *Cubic B-Spline Scheme*

The approximate solution $V(s,t)$ is constructed as:

$$V(s,t) = \sum_{j=-1}^{M+1} C_j(t) B_j(s), \tag{15}$$

where $C_j(t)$ are time-dependent coefficients and $B_j(s)$ are cubic B-spline (CuBS) basis functions [34]:

$$B_j(s) = \frac{1}{6h^3} \begin{cases} (s-s_j)^3, & s \in [s_j, s_{j+1}] \\ h^3 + 3h^2(s-s_{j+1}) & \\ +3h(s-s_{j+1})^2 - 3(s-s_{j+1})^3, & s \in [s_{j+1}, s_{j+2}] \\ h^3 + 3h^2(s_{j+3}-s) & \\ +3h(s_{j+3}-s)^2 - 3(s_{j+1}-s)^3, & s \in [s_{j+2}, s_{j+3}] \\ (s_{j+4}-s)^3, & s \in [s_{j+3}, s_{j+4}] \\ 0, & \text{otherwise.} \end{cases} \tag{16}$$

The set $\{B_{-3,4}, B_{-2,4}, \ldots, B_{M-2,4}, B_{M-1,4}\}$ forms a basis over $[a,b]$. Due to the local support property of cubic B-splines, only three non-zero basis functions $B_{j-3,4}(s)$, $B_{j-2,4}(s)$ and $B_{j-1,4}(s)$ contribute at the grid point (s_j, t^M). Thus the approximate solution at the M-th time level is given by:

$$v(s_j, t^m) = v_j^m = \sum_{w=j-1}^{j+1} C_w^m(t) B_w(s), \tag{17}$$

where C_j^m are time-dependent unknowns calculated using initial and boundary conditions. From (16) and (17), the approximate solutions and their derivatives are expressed in terms of C_j^m as:

$$\begin{cases} v_j^m = d_1 C_{j-1}^m + d_2 C_j^m + d_1 C_{j+1}^m, \\ (v_j^m)_s = -e_1 C_{j-1}^m + e_1 C_{j+1}^m, \\ (v_j^m)_{ss} = f_1 C_{j-1}^m + f_2 C_j^m + f_1 C_{j+1}^m, \end{cases} \tag{18}$$

where the coefficients are given by:

$$\begin{cases} d_1 = \dfrac{1}{6}, \quad d_2 = \dfrac{4}{6}, \\ e_1 = \dfrac{1}{2h}, \\ f_1 = \dfrac{1}{h^2}, \quad f_2 = -\dfrac{2}{h^2}. \end{cases} \tag{19}$$

The discretized form of (1) is:

$${}_0^{CF}\mathfrak{D}_t^{\gamma} v(s_j, t_{n+1}) = k(v_j^{n+1})_{ss} + a(v_j^{n+1}) - b(v_j^n)^q, \quad 0 < \gamma \leq 1. \tag{20}$$

For $n = 0$, we have

$$w_0 M_1^1 (v^1(x) - v^0) = k(v_j^1)_{ss} + a(v_j^1) - b(v_j^0)^q. \tag{21}$$

Using the CuBS approximation (18) in (21), we get:

$$\eta_5 C_{j-1}^1 + \eta_6 C_j^1 + \eta_5 C_{j+1}^1 = w_0 M_1^1 \left(d_1 C_{j-1}^0 + d_2 C_j^0 + d_1 C_{j+1}^0\right) - b\left(d_1 C_{j-1}^0 + d_2 C_j^0 + d_1 C_{j+1}^0\right)^q,$$

where $\eta_5 = w_0 M_1^1 d_1 - k f_1 - a d_1$ and $\eta_6 = w_0 M_1^1 d_2 - k f_2 - a d_2$.

In matrix form:

$$A_6 C^1 = w_0 M_1^1 A_7 C^0 - b(A_7 C^0)^q$$

where:

$$A_7 = \begin{bmatrix} d_1 & d_2 & d_1 & 0 & \dots & 0 \\ 0 & d_1 & d_2 & d_1 & \ddots & \vdots \\ \vdots & \ddots & \ddots & \ddots & \ddots & 0 \\ 0 & \dots & d_1 & d_2 & d_1 & 0 \\ 0 & \dots & 0 & d_1 & d_2 & d_1 \end{bmatrix}, \quad A_6 = \begin{bmatrix} \eta_5 & \eta_6 & \eta_5 & 0 & \dots & 0 \\ 0 & \eta_5 & \eta_6 & \eta_5 & \ddots & \vdots \\ \vdots & \ddots & \ddots & \ddots & \ddots & 0 \\ 0 & \dots & \eta_5 & \eta_6 & \eta_5 & 0 \\ 0 & \dots & 0 & \eta_5 & \eta_6 & \eta_5 \end{bmatrix}.$$

For $n \geq 1$, the scheme becomes:

$$w_0 \left[M_{n+1}^{n+1}(v^{n+1}(x) - v^n) + \sum_{j=1}^{n} (v^j(x) - v^{j-1}(x)) M_j^{n+1} \right] = k(v_j^{n+1})_{ss} + a(v_j^{n+1}) - b(v_j^n)^q.$$

Using the CuBS approximations (18), we obtain:

$$\begin{aligned} \eta_7 C_{j-1}^{n+1} + \eta_8 C_j^{n+1} + \eta_7 C_{j+1}^{n+1} &= w_0 M_{n+1}^{n+1} \left(d_1 C_{j-1}^n + d_2 C_j^n + d_1 C_{j+1}^n\right) \\ &- \sum_{j=1}^{n} M_j^{n+1} \left[\left(d_1 C_{j-1}^j + d_2 C_j^j + d_1 C_{j+1}^j\right) - \left(d_1 C_{j-1}^{j-1} + d_2 C_j^{j-1} + d_1 C_{j+1}^{j-1}\right) \right] \\ &- b\left(d_1 C_{j-1}^n + d_2 C_j^n + d_1 C_{j+1}^n\right)^q \end{aligned} \tag{22}$$

where $\eta_7 = w_0 M_{n+1}^{n+1} d_1 - k f_1 - a d_1$ and $\eta_8 = w_0 M_{n+1}^{n+1} d_2 - k f_2 - a d_2$.

In matrix form:

$$A_8 C^{n+1} = w_0 M_{n+1}^{n+1} A_7 C^n - b(A_7 C^n)^q - \sum_{j=1}^{n} (c^j(x) - c^{j-1}(x)) M_j^{n+1}$$

where:

$$A_8 = \begin{bmatrix} \eta_7 & \eta_8 & \eta_7 & 0 & \dots & 0 \\ 0 & \eta_7 & \eta_8 & \eta_7 & \ddots & \vdots \\ \vdots & \ddots & \ddots & \ddots & \ddots & 0 \\ 0 & \dots \eta_7 & \eta_8 & \eta_7 & 0 & \\ 0 & \dots & 0 & \eta_7 & \eta_8 & \eta_8 \end{bmatrix}.$$

The above system consists of $(M+1)$ equations involving $(M+3)$ unknowns. To ensure a unique solution, two additional equations are needed from the boundary conditions:

$$\begin{cases} \zeta_3 C_{-1}^{m+1} + \zeta_4 C_0^{m+1} + \zeta_3 C_1^{m+1} = 0, \\ \zeta_3 C_{M-1}^{m+1} + \zeta_4 C_M^{m+1} + \zeta_3 C_{M+1}^{m+1} = 0. \end{cases} \tag{23}$$

Combining (22) and (23) yields a nonlinear system of $(M+3)$ in $M+3$ unknowns C_{-1}^{n+1}, $C_0^{n+1}, \dots, C_{M+1}^{n+1}$, which can be solved using standard numerical techniques.

2.3 Extended Cubic B-Spline Scheme

An extended cubic B-Spline of degree four with a free parameter η is constructed by adding an extra term to the standard cubic B-Spline. The extended cubic B-Splines (ECuBS) basis functions, $EB_j^4(s,\eta)$ are given by:

$$EB_j^4(s,\eta) = \frac{1}{24h^4} \begin{cases} 4h(1-\eta)(s-s_j)^3 + 3\eta(s-s_j)^4, & s \in [s_j, s_{j+1}] \\ (4-\eta)h^4 + 12h^3(s-s_{j+1}) + 6h^2(2+\eta)(s-s_{j+1})^2 & \\ -12h(s-s_{j+1})^3 - 3\eta(s-s_{j+1})^4, & s \in [s_{j+1}, s_{j+2}] \\ (4-\eta)h^4 + 12h^3(s_{j+3}-s) + 6h^2(2+\eta)(s_{j+3}-s)^2 & \\ -12h(s_{j+3}-s)^3 - 3\eta(s_{j+1}-s)^4, & s \in [s_{j+2}, s_{j+3}] \\ 4h(1-\eta)(s_{j+4}-s)^3 + 3\eta(s_{j+4}-s)^4, & s \in [s_{j+3}, s_{j+4}] \\ 0, & \text{otherwise,} \end{cases} \tag{24}$$

where $\eta \in [-8, 1]$. Due to local support property, only $EB_{j-1}^4(s), EB_j^4(s)$ and $EB_{j+1}^4(s)$ contribute to the approximation at any point: support characteristic of the extended cubic B-splines so that the approximation v_j^m at the grid point (s_j, t_m) at m^{th} time level is given as

$$v(s_j, t^m) = v_j^m = \sum_{w=j-1}^{j+1} C_w^m(t) B_w^4(s,\eta). \tag{25}$$

The approximation and its derivatives are given by:

$$\begin{cases} v_j^m = g_1 C_{j-1}^m + g_2 C_j^m + g_1 C_{j+1}^m, \\ (v_j^m)_s = -h_1 C_{j-1}^m + h_1 C_{j+1}^m, \\ (v_j^m)_{ss} = i_1 C_{j-1}^m + i_2 C_j^m + i_1 C_{j+1}^m, \end{cases} \tag{26}$$

where the coefficients are:

$$g_1 = \frac{4-\eta}{24}, \quad g_2 = \frac{8+\eta}{12}, \quad h_1 = \frac{1}{2h}, \quad i_1 = \frac{2+\eta}{2h^2}, \quad i_2 = -\frac{2+\eta}{2h^2}.$$

Following the same procedure as before, for $n = 0$, the scheme becomes:

$$\begin{aligned} \eta_1' C_{j-1}^1 + \eta_2' C_j^1 + \eta_1' C_{j+1}^1 = w_0 M_1^1 \left[g_1 C_{j-1}^0 + g_2 C_j^0 + g_1 C_{j+1}^0 \right] \\ - b \left[g_1 C_{j-1}^0 + g_2 C_j^0 + g_1 C_{j+1}^0 \right]^q, \end{aligned} \tag{27}$$

where $\eta_1' = w_0 M_1^1 g_1 - k i_1 - a g_1$ and $\eta_2' = w_0 M_1^1 g_2 - k i_2 - a g_2$.

In matrix form:

$$A_6' C^1 = w_0 M_1^1 A_7' C^0 - b (A_7' C^0)^q,$$

with matrices defined as:

$$A_7' = \begin{bmatrix} g_1 & g_2 & g_1 & 0 & \cdots & 0 \\ 0 & g_1 & g_2 & g_1 & \ddots & \vdots \\ \vdots & \ddots & \ddots & \ddots & \ddots & 0 \\ 0 & \cdots & g_1 & g_2 & g_1 & 0 \\ 0 & \cdots & 0 & g_1 & g_2 & g_1 \end{bmatrix}, \quad A_6' = \begin{bmatrix} \eta_1' & \eta_2' & \eta_1' & 0 & \cdots & 0 \\ 0 & \eta_1' & \eta_2' & \eta_1' & \ddots & \vdots \\ \vdots & \ddots & \ddots & \ddots & \ddots & 0 \\ 0 & \cdots & \eta_1' & \eta_2' & \eta_1' & 0 \\ 0 & \cdots & 0 & \eta_1' & \eta_2' & \eta_1' \end{bmatrix}.$$

For $n \geq 1$, the scheme is:

$$\begin{aligned} \eta_3' C_{j-1}^{n+1} + \eta_4' C_j^{n+1} + \eta_3' C_{j+1}^{n+1} = w_0 M_{n+1}^{n+1} \left(g_1 C_{j-1}^n + g_2 C_j^n + g_1 C_{j+1}^n \right) \\ - \sum_{j=1}^{n} M_j^{n+1} \left[\left(g_1 C_{j-1}^j + g_2 C_j^j + g_1 C_{j+1}^j \right) \right. \\ \left. - \left(g_1 C_{j-1}^{j-1} + g_2 C_j^{j-1} + g_1 C_{j+1}^{j-1} \right) \right] \\ - b \left[g_1 C_{j-1}^n + g_2 C_j^n + g_1 C_{j+1}^n \right]^q, \end{aligned} \tag{28}$$

where $\eta_3' = w_0 M_{n+1}^{n+1} g_1 - k i_1 - a g_1$ and $\eta_4' = w_0 M_{n+1}^{n+1} g_2 - k i_2 - a g_2$.

The matrix form becomes:

$$A_8' C^n + 1 = w_0 M_{n+1}^{n+1} A_7' C^n - b (A_7' C^n)^q - \sum_{j=1}^{n} (c^j(x) - c^{j-1}(x)) M_j^{n+1}$$

with:

$$A_8' = \begin{bmatrix} \eta_7' & \eta_8' & \eta_7' & 0 & \dots & 0 \\ 0 & \eta_7' & \eta_8' & \eta_7' & \ddots & \vdots \\ \vdots & \ddots & \ddots & \ddots & \ddots & 0 \\ 0 & \dots \eta_7' & \eta_8' & \eta_7' & 0 & \\ 0 & \dots & 0 & \eta_7' & \eta_8' & \eta_8' \end{bmatrix}.$$

The system consists of $(M+1)$ equations with $(M+3)$ unknowns. The boundary conditions complete the system:

$$\begin{cases} \zeta_3' C_{-1}^{m+1} + \zeta_4' C_0^{m+1} + \zeta_3' C_1^{m+1} = 0, \\ \zeta_3' C_{M-1}^{m+1} + \zeta_4' C_M^{m+1} + \zeta_3' C_{M+1}^{m+1} = 0. \end{cases} \tag{29}$$

Combining (28) and (29) yields a $(M+3) \times (M+3)$ nonlinear system that can be solved for the unknown coefficients.

Remark 1: *A key advantage of ECuBS over its classical counterpart is the free parameter λ, which offers great flexibility in shaping the numerical solution and typically leads to improved accuracy. The standard cubic B-spline is reovered when $\lambda = 0$.*

Note on Notations: Throughout this paper, we employ the spatial variable s and fracitonal order parameter γ in place of the more conventional x and α. This deliberate choice in notation helps distinguish our work from existing literature while maintaining mathematical rigour. All symbols are explicitly defined to ensure clarity for the reader.

2.4 Initial State

To initiate the iteration procedure, it's crucial to determine the initial vector C^0 given by

$$C^0 = \left[C_{-1}^0, \quad C_0^0, \quad \dots \quad , C_M^0, \quad C_{M+1}^0\right]^T$$

The initial conditions for the problem are incorporated through the following set of equations:

$$\begin{cases} v_0' & = \phi'(s_0), \\ v_j^0 & = \phi(s_j), quadj = 0, 1, 2, 3, ..., M, \\ v_M' & = \phi'(s_M). \end{cases}$$

These equation specify the initial values and derivatives of the approximate solution for the initial time level ($m = 0$). Here, ϕ represents the initial function. This leads to the formulation of a system of $(M+3) \times (M+3)$ linear equations. This system can be written more compactly using matrix notation as:

$$A_5 C^0 = B_2,$$

where the matrices A_5, C^0 and B_2 are defined as:

$$A_5 = \begin{bmatrix} -\zeta_3 & \zeta_4 & \zeta_3 & 0 & \dots & 0 \\ \zeta_1 & \zeta_2 & \zeta_1 & 0 & \dots & 0 \\ 0 & \zeta_1 & \zeta_2 & \zeta_1 & \ddots & \vdots \\ \vdots & \ddots & \ddots & \ddots & \ddots & 0 \\ 0 & \dots & 0 & \zeta_1 & \zeta_2 & \zeta_1 \\ 0 & \dots & 0 & -\zeta_3 & \zeta_4 & \zeta_3 \end{bmatrix},$$

$$C^0 = \left[C^0_{-1}, \quad C^0_0 \quad , \dots , \quad C^0_M, \quad C^0_{M+1}\right]^T,$$

and

$$B_2 = \left[\phi'(s_0), \quad \phi(s_0) \quad , \dots , \quad \phi(s_M), \quad \phi'(s_M)\right]^T.$$

3 Stability Analysis

This section examines whether our trigonometric cubic B-spline method (11) stays stable. The same approach can be used to check stability for cubic and extended cubic B-spline methods too. Analyzing stability for nonlinear equations required careful treatment. We linearize Eq. (11) by setting $(v(s,t))^q = cv$, where c is a constant, following the approach of [35], and apply the von-Neumann method to obtain:

$$w_0\left[M^{n+1}_{n+1}(v^{n+1}(x) - v^n(x)) + w_0\sum_{r=1}^{n} M^{n+1}_r(v^r(x) - v^{r-1}(x))\right] = k(v^{n+1}_j)_{ss} + av^{n+1}_j - bcv^n_j. \tag{30}$$

This leads to the discretized form:

$$\begin{aligned} &\left[(w_0M^{n+1}_{n+1}a_1 - kc_1 - aa_1)C^{n+1}_{j-1} + (w_0M^{n+1}_{n+1}a_2 - kc_2 - aa_2)C^{n+1}_j\right. \\ &\quad \left. + (w_0M^{n+1}_{n+1}a_1 - kc_1 - aa_1)C^{n+1}_{j+1}\right] \\ &= (w_0M^{n+1}_{n+1} - bc)(a_1C^n_{j-1} + a_2C^n_j + a_1C^n_{j+1}) \\ &\quad - w_0\sum_{r=1}^{n} M^{n+1}_r\left[(a_1C^r_{j-1} + a_2C^r_j + a_1C^r_{j+1}) - (a_1C^{r-1}_{j-1} + a_2C^{r-1}_j + a_1C^{r-1}_{j+1})\right]. \end{aligned} \tag{31}$$

Let ρ^n_j be the exact growth factor and $\tilde{\rho}^n_j$ be its approximation. Defining the error $E^n_j = \rho^n_j - \tilde{\rho}^n_j$ yields:

$$\begin{aligned} &\left[(w_0M^{n+1}_{n+1}a_1 - kc_1 - aa_1)E^{n+1}_{j-1} + (w_0M^{n+1}_{n+1}a_2 - kc_2 - aa_2)E^{n+1}_j\right. \\ &\quad \left. + (w_0M^{n+1}_{n+1}a_1 - kc_1 - aa_1)E^{n+1}_{j+1}\right] \\ &= (w_0M^{n+1}_{n+1} - bc)(a_1E^n_{j-1} + a_2E^n_j + a_1E^n_{j+1}) \\ &\quad - w_0\sum_{r=1}^{n} M^{n+1}_r\left[(a_1E^r_{j-1} + a_2E^r_j + a_1E^r_{j+1}) - (a_1E^{r-1}_{j-1} + a_2E^{r-1}_j + a_1E^{r-1}_{j+1})\right]. \end{aligned} \tag{32}$$

The error satisfies the boundary and initial conditions:

$$E^n_0 = \psi_0(t^k), \qquad E^n_M = \psi_1(t^k), \qquad n = 0, 1, \dots, N \tag{33}$$

$$E_j^0 = \phi_0(x_j), \qquad (E_t)_j^0 = \phi_1(x_j), \qquad j = 1, 2, \ldots, M \tag{34}$$

Define the grid function:

$$E^n(x) = \begin{cases} E_j^n, & x_j - h/2 < x \le x_j + h/2,\ j = 1, \ldots, M-1 \\ 0, & \text{otherwise} \end{cases}$$

Its Fourier expansion is:

$$E^n(x) = \sum_{m=-\infty}^{\infty} \xi_n(m) e^{i2\pi mx/L},$$

where $\xi_n(m) = \dfrac{1}{b-a} \int_a^b E^n(x) e^{-i\dfrac{2\pi mx}{b-a}}\, dx$. Let $E^n = \begin{bmatrix} E_1^n & E_2^n & \ldots & E_{M-1}^n \end{bmatrix}^T$.

The L_2-norm on E^n is:

$$\|E^n\|_2 = \left(\sum_{j=1}^{M-1} h |E_j^n|^2 \right)^{\frac{1}{2}} = \left[\int_a^b |E^n(x)|^2\, dx \right]^{\frac{1}{2}}.$$

By Parseval identity, we have:

$$\int_a^b |E^n(x)|^2\, dx = \sum_{m=-\infty}^{\infty} |\xi_n(m)|^2,$$

which implies that

$$\|E^n\|_2^2 = \sum_{m=-\infty}^{\infty} |\xi_n(m)|^2. \tag{35}$$

Assume solutions of the form $E_j^n = \eta_n e^{i\beta js}$, where $i = \sqrt{-1}$ and $\beta \in [-\pi, \pi]$. Substituting into (32), dividing by $e^{i\beta js}$ and using the relation $e^{-i\beta s} + e^{i\beta s} = 2\cos(\beta s)$, we obtain:

$$\begin{aligned} &\left[2(w_0 M_{n+1}^{n+1} - a) a_1 \cos(\beta h) + (w_0 M_{n+1}^{n+1} - a) a_2 - k(2c_1 \cos(\beta h) + c_2) \right] \eta_{n+1} \\ &= (w_0 M_{n+1}^{n+1} - bc)(2a_1 \cos(\beta h) + a_2) \eta_n \\ &\quad - w_0 \sum_{r=1}^{n} M_r^{n+1} (2a_1 \cos(\beta h) + a_2)(\eta_r - \eta_{r-1}). \end{aligned}$$

For $\beta = 0$, this simplifies to:

$$\begin{aligned} &\left((w_0 M_{n+1}^{n+1} - a) - \frac{k(2c_1 + c_2)}{2a_1 + a_2} \right) \eta_{n+1} \\ &= (w_0 M_{n+1}^{n+1} - bc)\eta_n - w_0 \sum_{r=1}^{n} M_r^{n+1} (\eta_r - \eta_{r-1}). \end{aligned}$$

which can be written as:

$$\eta_{n+1} = \frac{d}{\zeta}\eta_n - \frac{w_0}{\zeta}\sum_{r=1}^{n} M_r^{n+1}(\eta_r - \eta_{r-1}), \tag{36}$$

where $d = (w_0 M_{n+1}^{n+1} - bc)$ and $\zeta = ((w_0 M_{n+1}^{n+1} - a) - \dfrac{k(2c_1 + c_2)}{2a_1 + a_2})$. Note that $2c_1 + c_2 = 0$, which implies $\zeta \geq 1$.

Proposition 1: *The growth factor η_n satisfies $|\eta_n| \leq D|\eta_0|$ for $n = 0, 1, 2, \ldots, N$, $D = |d|^2$.*

Proof: By mathematical induction:

- **Base case ($n = 0$):** Eq. (36) implies: $|\eta_1| \leq |d/\zeta||\eta_0| \leq |d|^2|\eta_0|$ since $\zeta \geq 1$.
- **Inductive step:** Assume $|\eta_k| \leq D|\eta_0|$ for $k \leq n$, then

$$\begin{aligned}
|\eta_{n+1}| &\leq \frac{|d|}{\zeta}|\eta_n| + \frac{w_0}{\zeta}\sum_{r=1}^{n} M_r^{n+1}(|\eta_r| - |\eta_{r-1}|) \\
&\leq |d|^2|\eta_0| - w_0|d|\sum_{r=1}^{n} M_r^{n+1}(|\eta_0| - |\eta_0|) \\
&= D|\eta_0|
\end{aligned}$$

where we have used the inequality $||a| - |b|| \leq |a - b|$ for $a, b \in \mathbb{R}$. □

Theorem 1: *The collocation scheme (11) is unconditionally stable.*

Proof: From Proposition 1 and Parseval's equality (35):

$$\|E_n\|_2^2 = \sum |\xi_n(m)|^2 \leq D^2 \sum |\xi_0(m)|^2 = D^2\|E_0\|_2^2.$$

Thus the scheme is unconditionally stable. □

4 Convergence Analysis

Temporal Convergece

This section derives convergence estimates for the cubic trigonometric B-spline scheme (11):

$$w_0\left[M_{n+1}^{n+1}(v^{n+1}(x) - v^n(x)) + \sum_{j=1}^{n}(v^j(x) - v^{j-1}(x))M_j^{n+1}\right] = k(v_j^{n+1})_{ss} + av_j^{n+1} - b(v_j^n)^q. \tag{37}$$

The analysis can be similarly extended to examine schemes using cubic and extended cubic B-splines.

We linearize the equation by setting $(v(s,t))^q = cv$, where c is a constant, yielding:

$$w_0\left[M_{n+1}^{n+1}(v^{n+1}(x) - v^n(x)) + \sum_{j=1}^{n}(v^j(x) - v^{j-1}(x))M_j^{n+1}\right] = k(v_j^{n+1})_{ss} + av_j^{n+1} - bcv_j^n. \tag{38}$$

Reformulating above equation yields:

$$(w_0M_{n+1}^{n+1}-a)v^{n+1}-k(v^{n+1})_{ss}=(w_0M_{n+1}^{n+1}-bc)v^n - w_0M_1^{n+1}(v^1-v^0)-w_0\sum_{j=2}^{n}(v^j-v^{j-1})M_j^{n+1}. \tag{39}$$

Theorem 2: *Let* $\{u(x,t^n)\}_{n=2}^N$ *be the analytical solution of Eq. (1) with initial and boundary conditions (2) and* $\{u^n\}_{n=2}^N$ *be the time discrete solution (39). The error estimate satisfies:*

$$\|e^{n+1}\| \le C\tau^{2-\gamma}$$

where $e^{n+1}=u(x,t^{n+1})-u^{n+1}$, $0<\gamma<1$ *and* C *is a constant.*

Proof: The exact solution satisfies the semi-discrete scheme (39) so that we have:

$$\begin{aligned}(w_0M_{n+1}^{n+1}-a)v(x,t^{n+1})-kv(x,t^{n+1})_{ss}&=(w_0M_{n+1}^{n+1}-bc)v(x,t^n)\\&-w_0M_1^{n+1}(v(x,t^1)-v(x,t^0))\\&-w_0\sum_{j=2}^{n}M_j^{n+1}[v(x,t^j)-v(x,t^{j-1})]+r_\tau^{n+1}.\end{aligned} \tag{40}$$

Subtracting (39) from (40) yields:

$$\begin{aligned}(w_0M_{n+1}^{n+1}-a)e^{n+1}-k(e^{n+1})_{xx}&=(w_0M_{n+1}^{n+1}-bc)e^n-w_0M_1^{n+1}e^1+w_0M_1^{n+1}e^0\\&-w_0\sum_{j=2}^{n}(e^j-e^{j-1})+r_\tau^{n+1}.\end{aligned} \tag{41}$$

Taking the inner product with e^{n+1} and using $e^0=0$:

$$\begin{aligned}(w_0M_{n+1}^{n+1}-a)\|e^{n+1}\|^2&=k\langle(e^{n+1})_{xx},e^{n+1}\rangle+(w_0M_{n+1}^{n+1}-bc)\langle e^n,e^{n+1}\rangle\\&-w_0M_1^{n+1}\langle e^1,e^{n+1}\rangle\\&-w_0\sum_{j=2}^{n}M_j^{n+1}\big(\langle e^j,e^{n+1}\rangle-\langle e^{j-1},e^{n+1}\rangle\big)\\&+\langle r_\tau^{n+1},e^{n+1}\rangle\\&=-k\|(e^{n+1})_x\|^2+(w_0M_{n+1}^{n+1}-bc)\langle e^n,e^{n+1}\rangle\\&-w_0M_1^{n+1}\langle e^1,e^{n+1}\rangle\\&-w_0\sum_{j=2}^{n}M_j^{n+1}\big(\langle e^j,e^{n+1}\rangle-\langle e^{j-1},e^{n+1}\rangle\big)\\&+\langle r_\tau^{n+1},e^{n+1}\rangle\\&\le(w_0M_{n+1}^{n+1}-bc)\langle e^n,e^{n+1}\rangle\end{aligned}$$

$$
\begin{aligned}
&- w_0 M_1^{n+1} \langle e^1, e^{n+1} \rangle \\
&- w_0 \sum_{j=2}^{n} M_j^{n+1} \left(\langle e^j, e^{n+1} \rangle - \langle e^{j-1}, e^{n+1} \rangle \right) \\
&+ \langle r_\tau^{n+1}, e^{n+1} \rangle
\end{aligned}
$$

where we have used $\langle u_{xx}, u \rangle = -\langle u_x, u_x \rangle$ and $||(e^{n+1})_x||^2 \geq 0$. Applying the Cauchy–Schwarz inequality:

$$
\left(w_0 M_{n+1}^{n+1} - a \right) ||e^{n+1}||^2 \leq \left(w_0 M_{n+1}^{n+1} - bc \right) \|e^n\| \|e^{n+1}\| - w_0 M_1^{n+1} \|e^1\| \|e^{n+1}\|
$$

$$
- w_0 \sum_{j=1}^{n-1} M_j^{n+1} (\|e^j\| \|e^{n+1}\| - \|e^{j-1}\| \|e^{n+1}\|) + \|r_\tau^{n+1}\| \|e^{n+1}\|
$$

which further simplifies to:

$$
\begin{aligned}
(w_0 M_{n+1}^{n+1} - a) \|e^{n+1}\| &\leq (w_0 M_{n+1}^{n+1} - bc) \|e^n\| - w_0 M_1^{n+1} \|e^1\| \\
&\quad - w_0 \sum_{j=2}^{n} M_j^{n+1} (\|e^j\| - \|e^{j-1}\|) + \|r_\tau^{n+1}\|.
\end{aligned}
$$

For $n = 0$:

$$
\|e^1\| \leq \frac{1}{w_0 M_1^1 - a + bc} \|r_\tau^1\| \leq C_0 \tau^{2-\gamma}.
$$

By induction, assume that $\|e^j\| \leq C\tau^{2-\gamma}$ for $j \leq q$. Then:

$$
\left(w_0 M_{q+1}^{q+1} - a \right) ||e^{q+1}|| \leq \left(w_0 M_{q+1}^{q+1} - bc \right) \|e^q\| - w_0 M_1^{q+1} \|e^1\|
$$

$$
- w_0 \sum_{j=2}^{q} M_j^{q+1} (\|e^j\| - \|e^{j-1}\|) + \|r_\tau^{q+1}\|
$$

Let $F = \max_{0 \leq i \leq q} ||e^i|| \leq C_1 \tau^{2-\gamma}$ and $G = \max_{0 \leq j \leq q} ||e^j|| - ||e^{j-1}|| \leq C_2 \tau^{2-\gamma}$. Then above inequality can be expressed as:

$$
\begin{aligned}
(w_0 M_{q+1}^{q+1} - a) \|e^{q+1}\| &\leq \Big[(w_0 M_{q+1}^{q+1} - bc) C_1 - w_0 M_1^{q+1} C_0 + C_u \\
&\quad - w_0 \sum_{j=2}^{q} M_j^{q+1} C_2 \Big] \tau^{2-\gamma}
\end{aligned}
$$

which implies:

$$
||e^{q+1}|| \leq C\tau^{2-\gamma},
$$

where $C = \dfrac{(w_0 M_{q+1}^{q+1} - bc) C_1 - w_0 M_1^{q+1} C_0 + C_u - w_0 \sum_{j=2}^{q} M_j^{q+1} C_2}{w_0 M_{q+1}^{q+1} - a}$.

This completes the proof. □

Spatial Convergence

The methodology described in [35] is employed to examine the convergence of the proposed numerical scheme. We begin with the following fundamental convergence theorem:

Lemma 3: *The set* $\{T_{-3,4}, T_{-2,4}, \ldots, T_{M-1,4}\}$ *of trignometric B-spline basis functions of order 4 satisfies the inequality:*

$$\sum_{j=-3}^{M-1} \left|T_{j,4}(x)\right| \leq K, \quad \forall x \in [a,b], \tag{42}$$

where $[a,b]$ *is the approximation domain and the coefficients satisfy* $2a_1 + a_2 = 1$ *and* $2c_1 + c_2 = 0$*. Here* K *is an arbitrary positive constant*.

Proof: We prove this resutl by examining the number and structure of nonzero basis functions at any fixed $x \in [a,b]$, taking into account the local support property of the cubic trigonometric B-splines.

Case 1: At knots $x = x_j$ Due to the local support property of B-spline basis functions of order 4, exactly three B-splines overlap at each knot x_j:

$$\sum_{k=-3}^{M-1} |T_{k,4}(x_j)| = |T_{j-3,4}(x_j)| + |T_{j-2,4}(x_j)| + |T_{j-1,4}(x_j)|$$

$$= a_1 + a_2 + a_1 = 2a_1 + a_2 = 1 < K.$$

Case 2: Between knots $x \in (x_j, x_{j+1})$

$$\sum_{k=-3}^{M-1} |T_{k,4}(x)| \leq a_1 + a_2 + a_2 + a_1 = 2a_1 + 2a_2$$

$$= (2a_1 + a_2) + a_2 = 1 + a_2 \leq K$$

Boundary Cases: At the domain boundaries $x = a$ and $x = b$, fewer than four basis functions are non-zero. Therefore,

$$\sum_{j=-3}^{M-1} |T_{j,4}(x)| \leq K, \quad \forall x \in [a,b]. \tag{43}$$

Hence, the inequality holds forany positive constant K which completes the proof. □

Theorem 3: *Let* $q \in C^2[a,b]$ *and suppose* $u(x,t) \in C^4[a,b] \times C^2[0,\infty)$*. Consider a uniform partition of* $[a,b]$*,* $\chi = \{a = x_0 < x_1 < \cdots < x_{M-1} < x_M = b\}$ *with* $x_j = a + jh$ *for* $j = 0, 1, \ldots, M$*, where* $h = (b-a)/M$*. Let* $\widetilde{U}(x,t)$ *denote the unique spline that interpolates* $u(x,t)$ *at the nodes* $x_j \in \chi$*. Then for every* $t \geq 0$*, there exist constants* $\rho_j > 0$ *independent of* h *such that for* $j = 0, 1, 2$*,*

$$\|D^j(u(x,t) - \widetilde{U}(x,t))\|_\infty \leq \rho_j h^{4-j} \tag{44}$$

Theorem 4: *The numerical solution* $U(x,t)$ *converges to the exact solution* $u(x,t)$ *of NWSE. Furthermore, if* $q \in C^2[a,b]$*, then there exists a constant* $\widetilde{\rho} > 0$ *independent of the mesh size* h *such that for all* $t \geq 0$*,*

$$\|u(x,t) - U(x,t)\|_\infty \leq \widetilde{\rho} h^2 \tag{45}$$

provided that h is sufficiently small.

Proof: Let $\widetilde{U}(x,t) = \sum_{j=-3}^{M-1} d_j(t) T_{j,4}(x)$ be the trignometric B-spline approximation of $U(x,t)$. By the triangle inequality,

$$\|u(x,t) - U(x,t)\|_\infty \leq \|u(x,t) - \widetilde{U}(x,t)\|_\infty + \|\widetilde{U}(x,t) - U(x,t)\|_\infty \tag{46}$$

From Theorem 3 with $j = 0$, we have

$$\|u(x,t) - \widetilde{U}(x,t)\|_\infty \leq \rho_0 h^4. \tag{47}$$

For the discretization error $e(x,t) = \widetilde{U} - U$, consider the collocation equations at the nodes:

$$Lu(x_j,t) = f(x_j,t), L\widetilde{U} = f(x_j,t) + \tau_j(t),$$

where the spatial truncation error satisfies $|\tau_j\|_\infty \leq C_\tau h^2$ due to the approximation peoperties of the B-spline.

The error equation at the spatial nodes is:

$$\begin{aligned}\left[(w_0 M_{n+1}^{n+1} - a)(2a_1 + a_1) - k(2c_1 + c_2)\right] e_j^{n+1} = (w_0 M_{n+1}^{n+1} - bc)(c_1 e_{j-1}^n + c_2 e_j^n + c_1 e_{j+1}^n) \\ - w_0 \sum_{r=1}^{n} M_r^{n+1} \triangle^2 e_j^{r-k} + \tau_j^{n+1},\end{aligned} \tag{48}$$

where $\triangle^2 e_j^n = e_j^n - e_j^{n-1}$ and $\|\tau_j^{n+1}\|_\infty \leq C_\tau h^2$. Using $2a_1 + a_2 = 1$, $2c_1 + c_2 = 0$, and defining $\Gamma = (w_0 M_{n+1}^{n+1} - a) > 0$:

$$\Gamma \|e^{n+1}\|_\infty \leq (w_0 M_{n+1}^{n+1} - bc)\|e^n\|_\infty + w_0 \sum_{r=1}^{n} M_r^{n+1} \|\triangle^2 e_j^{r-k}\|_\infty + C_\tau h^2. \tag{49}$$

Base Case (n = 0):

$$\Gamma \|e^1\|_\infty \leq C_\tau h^2 \Rightarrow \|e^1\|_\infty \leq \frac{C_\tau h^2}{\Gamma}.$$

Inductive Step: Assume that $\|e^k\|_\infty \leq \rho h^2$ holds for $k \leq n$. Then: From Eq. (49), taking absolute values and using the inductive hypothesis:

$$\Gamma \|e^1\|_\infty \leq \left[(w_0 M_{n+1}^{n+1} - bc) + 2w_0 \sum_{r=1}^{n} M_r^{n+1}\right] \rho h^2 + C_\tau h^2. \tag{50}$$

Since $\sum_{r=1}^{n} M_r^{n+1} \leq M_{n+1}^{n+1} by the properties of M_r$, we obtain:

$$\|e^{n+1}\| \leq \left[\frac{(3w_0 M_{n+1}^{n+1} - bc)\rho + C_\tau}{\Gamma}\right] h^2. \tag{51}$$

Choose ρ large enough so that $\frac{(3w_0 M_{n+1}^{n+1} - bc)\rho + C_\tau}{\Gamma} \leq \rho$ yield uniform boundedness.

By the Lemma (3) and the boundedness of the basis:

$$\|\widetilde{U} - U\|_\infty \leq K\rho h^2. \tag{52}$$

Combining (47) and (52):

$$\|u(x,t) - U(x,t)\|_\infty \leq \rho_0 h^4 + K\rho h^2 \leq \widetilde{\rho} h^2, \tag{53}$$

where $\widetilde{\rho} = \rho_0 h_0^2 + K\rho$ for $h < h_0$, which complete the proof. □

5 Numerical Experiments

This section aims to validate and evaluate the effectiveness of the proposed methodology by employing a range of test problems and utilizing error norms. We compare the numerical results obtained from our proposed scheme with those from [1]. All numerical computations and visualizations were performed using Mathematica 13.2. All simulations were executed on a window 10 (64-bit) workstation equipped with an Intel Core i5 processor and 32 GB of system memory. We employ the following error measures:

- Absolute error
- L_∞ error norm

The absolute error is positive difference between the exact solution u^{ext} and the numerical approximation U^{app} at each grid point.

$$\text{Absolute Error} = \left|u^{\text{ext}}(x_i) - U^{\text{app}}(x_i)\right| \qquad \forall \quad x_i \in [a,b]$$

The error norms are defined as:

$$L_\infty = \max_{0\leq i\leq M} \left|u^{\text{ext}}(x_i) - U^{\text{app}}(x_i)\right| \qquad \forall \quad x_i \in [a,b]$$

Here $u^{\text{ext}}(x_i)$ and $U^{\text{app}}(x_i)$ represent the exact and approximate solutions at fixed time t, respectively. The convergence rate for spatial step size h is given by [36]:

$$p_h = \frac{\log\left(\frac{\mathcal{E}(h_1)-\mathcal{E}(h_2)}{\mathcal{E}(h_2)-\mathcal{E}(h_3)}\right)}{\log\left(\frac{h_2}{h_1}\right)}, \quad \textit{where} \quad h_1 > h_2. \tag{54}$$

For temporal step size Δt:

$$p_{\Delta t} = \frac{\log\left(\frac{\mathcal{E}(\Delta t_1)-\mathcal{E}(\Delta t_2)}{\mathcal{E}(\Delta t_2)-\mathcal{E}(\Delta t_3)}\right)}{\log\left(\frac{\Delta t_2}{\Delta t_1}\right)}, \quad \textit{where} \quad \Delta t_1 > \Delta t_2, \tag{55}$$

where $\mathcal{E}$ denotes error norm L_∞.

Example 1: *[1] Consider the time fractional NWS model:*

$$\frac{\partial^\gamma v(s,t)}{\partial t^\gamma} = \frac{\partial^2 v(s,t)}{\partial s^2} - 2v(s,t), \quad 0 < \gamma \leq 1,\ s \in \Omega,\ t \geq 0,$$

with ICs:

$$v(s,0) = e^{s},$$

and BCs:

$$v(0,t) = 0, \quad v(1,t) = 0, \quad t > 0.$$

We apply the proposed numerical scheme to solve this example. Tables 1–3 present detailed quantitiative comparisons of our obtained results using different spline methods (TCuBS, CuBS and ECuBS) against the exact solution for the integer order case ($\gamma = 1$) [1]. These tables reveal the accuracy of the scheme at various fractional orders ($\gamma = 0.9, 0.75, 0.5$) and across different spatial points $s \in [0,1]$. Fig. 1 shows a visual comparison between the approximate solutions at different values of γ using TCuBS. Fig. 2 shows a visual comparison between the approximate solutions at different values of t using TCuBS. Table 4 gives comparision of absolute error of TCuBS and four term solution at $\gamma = 0.9$. Table 5 gives spital convergence at different values of M. Table 6 gives temporal convergence at different values of τ. Fig. 3 illustrates 3D approximate solutions at different values of γ using TCuBS. The approximate solution with $M = 80$, $\tau = 0.01$ and $t = 1$ is given by:

$$V(s,1) = \begin{cases} 0.413898\cos\left(\frac{s}{2}\right) - 0.0460185\cos\left(\frac{3s}{2}\right) + 2.00941\sin\left(\frac{s}{2}\right) - 0.296075\sin\left(\frac{3s}{2}\right), & s \in [0, \frac{1}{20}) \\ 0.415258\cos\left(\frac{s}{2}\right) - 0.0473772\cos\left(\frac{3s}{2}\right) + 1.95503\sin\left(\frac{s}{2}\right) - 0.277993\sin\left(\frac{3s}{2}\right), & s \in [\frac{1}{20}, \frac{1}{10}) \\ 0.4176\cos\left(\frac{s}{2}\right) - 0.0497112\cos\left(\frac{3s}{2}\right) + 1.90823\sin\left(\frac{s}{2}\right) - 0.26255\sin\left(\frac{3s}{2}\right), & s \in [\frac{1}{10}, \frac{3}{20}) \\ \vdots & \vdots \\ 0.62181\cos\left(\frac{s}{2}\right) - 0.222638\cos\left(\frac{3s}{2}\right) + 1.22904\sin\left(\frac{s}{2}\right) - 0.119448\sin\left(\frac{3s}{2}\right), & s \in [\frac{17}{20}, \frac{9}{10}) \\ 0.675575\cos\left(\frac{s}{2}\right) - 0.26284\cos\left(\frac{3s}{2}\right) + 1.11773\sin\left(\frac{s}{2}\right) - 0.110424\sin\left(\frac{3s}{2}\right), & s \in [\frac{9}{10}, \frac{19}{20}) \\ 0.742395\cos\left(\frac{s}{2}\right) - 0.311025\cos\left(\frac{3s}{2}\right) + 0.987803\sin\left(\frac{s}{2}\right) - 0.103349\sin\left(\frac{3s}{2}\right), & s \in [\frac{19}{20}, 1] \end{cases}$$

Example 2: *[1] Consider the time-fractional NWS model:*

$$\frac{\partial^{\gamma} v(s,t)}{\partial t^{\gamma}} = \frac{\partial^2 v(s,t)}{\partial s^2} + 3v(s,t) - 4v(s,t)^3, \quad 0 < \gamma \leq 1,\ s \in \Omega,\ t \geq 0,$$

with ICs:

$$v(s,0) = \sqrt{\frac{3}{4}} \frac{e^{\sqrt{6}s}}{e^{\sqrt{6}s} + exp^{\frac{\sqrt{6}}{2}s}}, \quad 0 \leqslant s \leqslant 1,$$

and BCs:

$$v(0,t) = 0, \quad v(1,t) = 0, \quad t > 0,$$

and nonlinear term:

$$f(v) = v^3.$$

Table 1: Comparison of approximate solutions using various splines when $\gamma = 0.9, \tau = 0.01$, $t = 1$ for Example 1

s	TuBS	CuBS	ECuBS	4 term solution [1]	Exact when $\gamma = 1$
0.1	0.411731	0.411741	0.418010	0.358075	0.406570
0.2	0.458745	0.458746	0.470220	0.395734	0.449329
0.3	0.509309	0.509321	0.524861	0.437354	0.496585
0.4	0.563829	0.563920	0.582152	0.483351	0.548812
0.5	0.622737	0.622841	0.642450	0.534186	0.606531
0.6	0.686487	0.686560	0.706051	0.590366	0.670321
0.7	0.75556	0.755630	0.773241	0.652456	0.740818
0.8	0.830466	0.830571	0.844450	0.721075	0.818731
0.9	0.911751	0.911851	0.919830	0.796911	0.904837

Table 2: Comparison of approximate solutions using various splines when $\gamma = 0.75, \tau = 0.01$, $t = 1$ for Example 1

s	TuBS	CuBS	ECuBS	4 term solution [1]	Exact when $\gamma = 1$
0.1	0.419672	0.419731	0.423850	0.310829	0.40657
0.2	0.473039	0.473051	0.480741	0.343552	0.449329
0.3	0.528486	0.528551	0.539040	0.379648	0.496585
0.4	0.586443	0.586470	0.598961	0.419576	0.548812
0.5	0.647260	0.647350	0.660530	0.463703	0.606531
0.6	0.711207	0.7112501	0.724250	0.512471	0.67032
0.7	0.778455	0.778541	0.789950	0.566368	0.740818
0.8	0.849069	0.849160	0.857951	0.625933	0.818731
0.9	0.922989	0.923051	0.928060	0.691763	0.904837

Table 3: Comparison of approximate solutions using various splines when $\gamma = 0.5, \tau = 0.01$, $t = 1$ for Example 1

s	TuBS	CuBS	ECuBS	4 term solution [1]	Exact when $\gamma = 1$
0.1	0.424061	0.42416	0.42662	0.184195	0.40657
0.2	0.480938	0.48094	0.48584	0.203567	0.449329
0.3	0.539081	0.53918	0.54586	0.224976	0.496585
0.4	0.598932	0.59894	0.60694	0.248637	0.548812
0.5	0.660798	0.66087	0.66925	0.274787	0.606531
0.6	0.724845	0.72485	0.73307	0.303686	0.670332
0.7	0.791081	0.79112	0.79824	0.335625	0.740818

(Continued)

Table 3 (continued)

s	TuBS	CuBS	ECuBS	4 term solution [1]	Exact when $\gamma = 1$
0.8	0.859328	0.85933	0.86467	0.370923	0.818731
0.9	0.929188	0.92922	0.93204	0.409934	0.904837

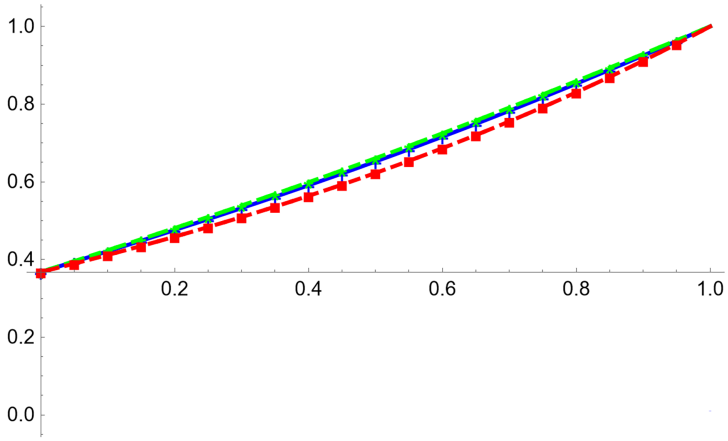

Figure 1: Comparison of the approximate solution at different values of γ using TCuBS when $h = \frac{1}{80}, \tau = 0.01, t = 1$

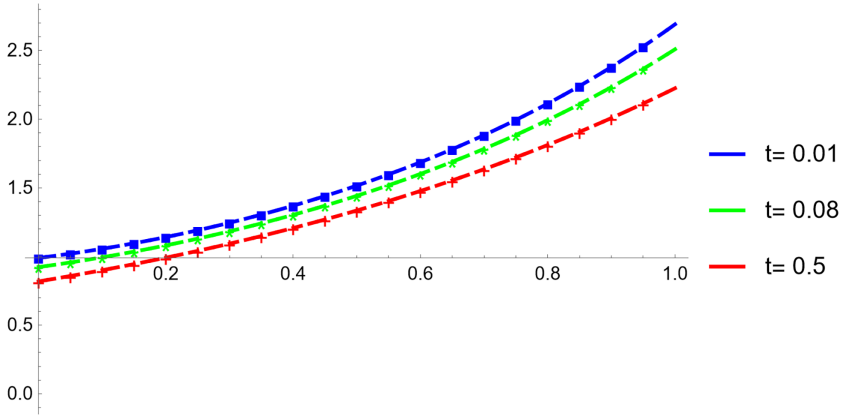

Figure 2: Comparison of the approximate solution at different values of t using TCuBS when $h = \frac{1}{80}, \tau = 0.01, \gamma = 0.8$

Table 4: Comparison of absolute error using trignometric B spline with absolute error of first three terms solutions when $\gamma = 0.9, \tau = 0.01, t = 1$ for Example 1

s	TuBS	4 term solution [1]	Exact when $\gamma = 1$	Absolute error [1]	Absolute error TuBS
0.1	0.411731	0.358075	0.406570	0.048495	0.005161
0.2	0.458745	0.395734	0.449329	0.009416	0.004160
0.3	0.509309	0.437354	0.496585	0.059235	0.012724
0.4	0.563829	0.483351	0.548812	0.065461	0.015017
0.5	0.622737	0.534186	0.606531	0.072345	0.016202
0.6	0.686487	0.590366	0.670321	0.079955	0.016166
0.7	0.755560	0.652456	0.740818	0.088362	0.014742
0.8	0.830466	0.721075	0.818731	0.097656	0.011735
0.9	0.911751	0.796911	0.904837	0.107926	0.006914

Table 5: Spatial convergence corresponding L_∞ error at different values of M for Example 1 at time $t = 1$, $\tau = \frac{1}{100}$ and $\gamma = 0.9$

M	L_∞ Error	p_h
10	3.05081×10^{-3}	————
20	2.88750×10^{-3}	2.0000
40	2.84683×10^{-3}	1.9916
80	2.83660×10^{-3}	2.04439
160	2.83412×10^{-3}	—————

Table 6: Temporal convergence corresponding L_∞ error at different values of τ for Example 1 at time $t = 1$, $M = 20$ and $\gamma = 0.9$

τ	L_∞ Error	$p_{\Delta t}$
$\frac{1}{10}$	2.20565×10^{-2}	————
$\frac{1}{20}$	8.50420×10^{-3}	2.00000
$\frac{1}{40}$	2.97733×10^{-3}	1.65530
$\frac{1}{80}$	1.22271×10^{-3}	1.85220
$\frac{1}{160}$	7.37809×10^{-4}	—————

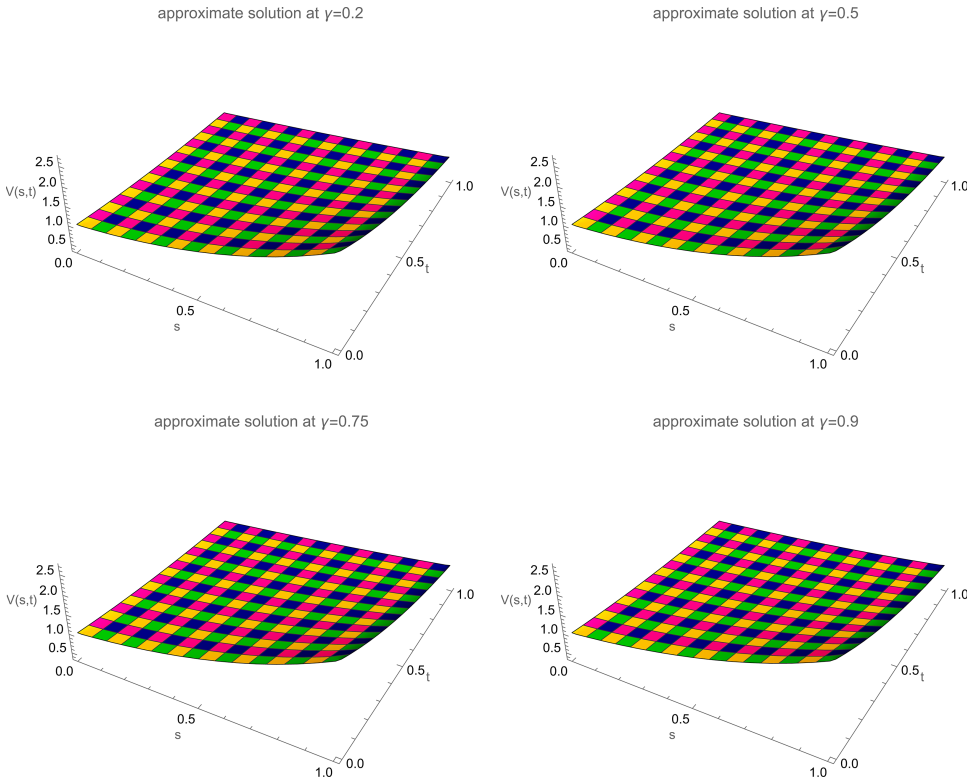

Figure 3: 3D comparison of approximate solutions at various γ using TCuBS when $h = \frac{1}{80}, \tau = 0.01$, $T = 1$

We apply the proposed numerical scheme is to solve this example. Tables 7–9 present comprehensive numerical comparisons of our results obtained using different spline methods (TCuBS, CuBS and ECuBS) against the exact solution for the integer-order case ($\gamma = 1$). These tables quantitatively demonstrate the accuracy of our method across different fractioal orders ($\gamma = 0.9, 0.75, 0.5$) and spatial locations showing particularly good agreement with the exact solution while mantaining the computational efficiency. Table 10 gives comparision of absolute error of TCuBS and four term solution at $\gamma = 0.9$. Table 11 gives spatial convergence at different values of M. Table 12 gives temporal convergence at different values of τ. Fig. 4 shows a visual comparison between the approximate solutions at different values of γ using TCuBS. Fig. 5 shows a visual comparison between the approximate solutions at different values of t using TCuBS. Fig. 6 presents 3D visualization of the approximate solutions at various γ values using TCuBS, demonstrating the spatiotemporal behavior of the solutions. The approximate solution with $M = 80$, $\tau = 0.01$ and $t = 1$ is given as:

$$V(s,1)=\begin{cases}0.966166\cos\left(\frac{s}{2}\right)-0.109655\cos\left(\frac{3s}{2}\right)-0.061874\sin\left(\frac{s}{2}\right)+0.0352843\sin\left(\frac{3s}{2}\right), & s\in\left[0,\frac{1}{20}\right)\\ 0.965056\cos\left(\frac{s}{2}\right)-0.108546\cos\left(\frac{3s}{2}\right)-0.0174789\sin\left(\frac{s}{2}\right)+0.0205229\sin\left(\frac{3s}{2}\right), & s\in\left[\frac{1}{20},\frac{1}{10}\right)\\ 0.963151\cos\left(\frac{s}{2}\right)-0.106648\cos\left(\frac{3s}{2}\right)+0.0205828\sin\left(\frac{s}{2}\right)+0.00796241\sin\left(\frac{3s}{2}\right), & s\in\left[\frac{1}{10},\frac{3}{20}\right)\\ \vdots & \vdots\\ 0.998012\cos\left(\frac{s}{2}\right)-0.132853\cos\left(\frac{3s}{2}\right)+0.0123645\sin\left(\frac{s}{2}\right)+0.00917574\sin\left(\frac{3s}{2}\right), & s\in\left[\frac{17}{20},\frac{9}{10}\right)\\ 1.01524\cos\left(\frac{s}{2}\right)-0.145737\cos\left(\frac{3s}{2}\right)-0.023305\sin\left(\frac{s}{2}\right)-0.00628389\sin\left(\frac{3s}{2}\right), & s\in\left[\frac{9}{10},\frac{19}{20}\right)\\ 1.03631\cos\left(\frac{s}{2}\right)-0.160931\cos\left(\frac{3s}{2}\right)-0.0642746\sin\left(\frac{s}{2}\right)-0.00405288\sin\left(\frac{3s}{2}\right), & s\in\left[\frac{19}{20},1\right]\end{cases}$$

Table 7: Comparison of the approximate solutions using various splines when $\gamma = 0.9$, $\tau = 0.01$, $t = 1$ for Example 2

s	TuBS	CuBS	ECuBS	4 term solution [1]	Exact when $\gamma = 1$
0.1	0.866541	0.86653	0.86432	1.46487	0.857597
0.2	0.873867	0.87391	0.87023	1.47719	0.85856
0.3	0.879897	0.87907	0.87441	1.48288	0.859414
0.4	0.882178	0.88234	0.87715	1.48207	0.860171
0.5	0.883681	0.88372	0.87853	1.47514	0.860842
0.6	0.883543	0.88353	0.87854	1.46262	0.861436
0.7	0.881697	0.88174	0.87710	1.44518	0.861963
0.8	0.877948	0.87793	0.87423	1.42360	0.862429
0.9	0.871954	0.87193	0.86970	1.39869	0.862842

Table 8: Comparison of the approximate solutions using various splines when $\gamma = 0.75, \tau = 0.01$, $t = 1$ for Example 2

s	TuBS	CuBS	ECuBS	4 term solution [1]	Exact when $\gamma = 1$
0.1	0.863014	0.86302	0.85884	1.51075	0.857597
0.2	0.868119	0.86812	0.86105	1.52185	0.85856
0.3	0.871978	0.87202	0.86306	1.52621	0.859414
0.4	0.874683	0.87472	0.86478	1.52394	0.860171
0.5	0.876262	0.87633	0.86604	1.51541	0.860842
0.6	0.876678	0.87678	0.86693	1.50115	0.861436
0.7	0.875823	0.87584	0.86724	1.48186	0.861963
0.8	0.873506	0.87353	0.86682	1.45832	0.862429
0.9	80.869437	0.86944	0.86555	1.43136	0.862842

Table 9: Comparison of the approximate solutions using various splines when $\gamma = 0.5, \tau = 0.01$, $t = 1$ for Example 2

s	TuBS	CuBS	ECuBS	4 term solution [1]	Exact when $\gamma = 1$
0.1	0.858616	0.85862	0.85881	1.54829	0.857597
0.2	0.860720	0.86073	0.86102	1.55782	0.85856
0.3	0.862672	0.86268	0.86302	1.56071	0.859414
0.4	0.864337	0.86435	0.86472	1.55701	0.860171
0.5	0.865795	0.86582	0.86603	1.54701	0.860842
0.6	0.866863	0.86692	0.86694	1.53125	0.861436
0.7	0.867387	0.86743	0.86723	1.51041	0.861963
0.8	0.867154	0.86724	0.86680	1.48528	0.862429
0.9	0.865882	0.86593	0.86551	1.45670	0.862842

Table 10: Comparison of absolute error using trignometric B spline with absolute error of first three terms solutions when $\gamma = 0.9, \tau = 0.01, t = 1$ for Example 2

s	TuBS	4 term solution [1]	Exact when $\gamma = 1$	Absolute error [1]	Absolute error TuBS
0.1	0.866541	1.46487	0.857597	0.607273	0.008944
0.2	0.873867	1.47719	0.858560	0.618630	0.015307
0.3	0.879897	1.48288	0.859414	0.623466	0.020483
0.4	0.882178	1.48207	0.860171	0.621899	0.022007
0.5	0.883681	1.47514	0.860842	0.614298	0.022839
0.6	0.883543	1.46262	0.861436	0.601184	0.022107
0.7	0.881697	1.44518	0.861963	0.583217	0.019734
0.8	0.877948	1.42360	0.862429	0.561171	0.015519
0.9	0.871954	1.39869	0.862842	0.536270	0.009534

Table 11: Spatial convergence corresponding L_∞ error at different values of M for Example 2 at time $t = 1$, $\tau = \frac{1}{100}$ and $\gamma = 0.9$

M	L_∞ Error	p_h
10	1.45731×10^{-6}	————
20	3.63490×10^{-7}	2.0000
40	9.08195×10^{-8}	2.0000
80	2.27015×10^{-8}	1.97990
160	5.67518×10^{-9}	—————

Table 12: Temporal convergence corresponding L_∞ error at different values of τ for Example 2 at time $t = 1$, $M = 20$ and $\gamma = 0.9$

τ	L_∞ Error	$p_{\Delta t}$
$\frac{1}{10}$	3.54840×10^{-6}	————
$\frac{1}{20}$	1.76043×10^{-6}	2.003320
$\frac{1}{40}$	8.44685×10^{-7}	2.000842
$\frac{1}{80}$	3.81215×10^{-7}	2.000215
$\frac{1}{160}$	1.48061×10^{-7}	—————

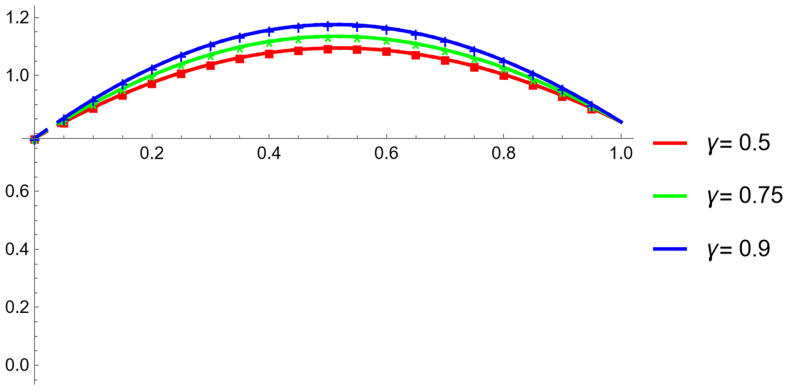

Figure 4: Comparison of the approximate solution at different values of γ using TCuBS when $h = \frac{1}{80}, \tau = 0.01, t = 1$

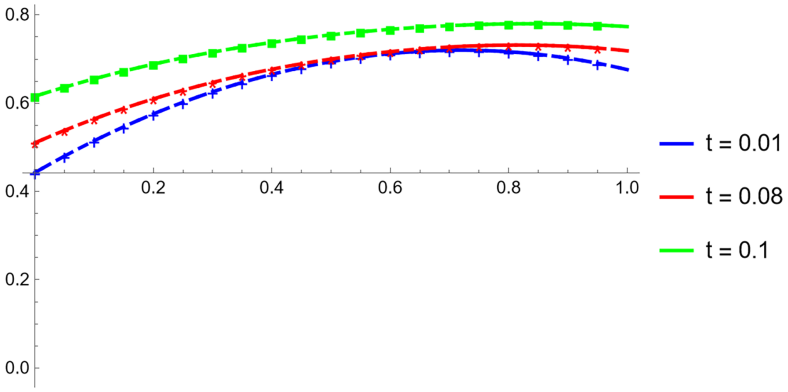

Figure 5: Comparison of the approximate solution at different values of t using TCuBS when $h = \frac{1}{80}, \tau = 0.01, \gamma = 0.8$

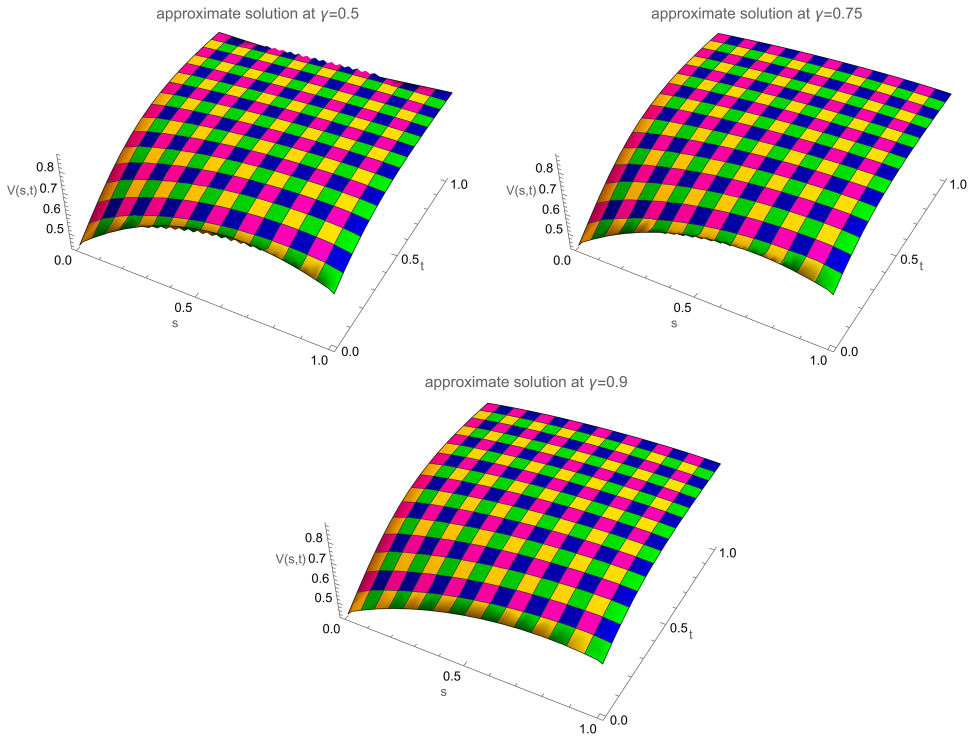

Figure 6: 3D approximate solutions for Example 2 at different γ using TCuBS when $h = \frac{1}{80}$, $\tau = 0.01$, and $t = 1$

Example 3: *[1] Consider the time-fractional NWS model:*

$$\frac{\partial^\gamma v(s,t)}{\partial t^\gamma} = \frac{\partial^2 v(s,t)}{\partial s^2} + v(s,t) - v(s,t)^2, 0 < \gamma \leq 1, s \in \Omega, t \geq 0,$$

with ICs:

$$v(s,0) = \frac{1}{(1+e^{\frac{s}{\sqrt{6}}})^2}$$

BCs:

$$v(0,t) = 0, \quad v(1,t) = 0, \quad t > 0,$$

and nonlinear term:

$$f(v) = v^2.$$

We apply the proposed numerical scheme is to solve this example. Tables 13–15 provide detailed numerical comparisons between our results using different spline methods (TCuBS, CuBS and ECuBS) against the exact solution for the integer-order case ($\gamma = 1$). These tables quantitatively access the accuracy of our method across different fractional orders ($\gamma = 0.9, 0.75, 0.5$) and spatial locations showing excellent agrement with the exact solution. Table 16 gives comparision of absolute error of TCuBS and four term solution at $\gamma = 0.9$. Table 17 gives spital convergence at different

values of M. Table 18 gives temporal convergence at different values of τ. Fig. 7 presents a comparison of approximate solutions at different values of γ using TCuBS. Fig. 8 presents a comparison of approximate solutions at different values of t using TCuBS. Fig. 9 shows 3D visualization of the approximate solutions at various γ values using TCuBS. The approximate solution with $M = 80$, $\tau = 0.01$ and $T = 1$ is given by:

$$V(s,1) = \begin{cases} 0.571478\cos\left(\frac{s}{2}\right) - 0.0855868\cos\left(\frac{3s}{2}\right) - 0.373819\sin\left(\frac{s}{2}\right) + 0.0326049\sin\left(\frac{3s}{2}\right), & s \in [0, \frac{1}{20}) \\ 0.5708\cos\left(\frac{s}{2}\right) - 0.0849086\cos\left(\frac{3s}{2}\right) - 0.346676\sin\left(\frac{s}{2}\right) + 0.0235798\sin\left(\frac{3s}{2}\right), & s \in [\frac{1}{20}, \frac{1}{10}) \\ 0.569495\cos\left(\frac{s}{2}\right) - 0.0836081\cos\left(\frac{3s}{2}\right) - 0.3206\sin\left(\frac{s}{2}\right) + 0.0149745\sin\left(\frac{3s}{2}\right), & s \in [\frac{1}{10}, \frac{3}{20}) \\ \vdots & \vdots \\ 0.493297\cos\left(\frac{s}{2}\right) - 0.0165519\cos\left(\frac{3s}{2}\right) - 0.0110574\sin\left(\frac{s}{2}\right) - 0.0609313\sin\left(\frac{3s}{2}\right), & s \in [\frac{17}{20}, \frac{9}{10}) \\ 0.484777\cos\left(\frac{s}{2}\right) - 0.0101816\cos\left(\frac{3s}{2}\right) + 0.00657908\sin\left(\frac{s}{2}\right) - 0.0623612\sin\left(\frac{3s}{2}\right), & s \in [\frac{9}{10}, \frac{19}{20}) \\ 0.475777\cos\left(\frac{s}{2}\right) - 0.0036914\cos\left(\frac{3s}{2}\right) + 0.0240798\sin\left(\frac{s}{2}\right) - 0.0633142\sin\left(\frac{3s}{2}\right), & s \in [\frac{19}{20}, 1] \end{cases}$$

Table 13: Comparison of approximate solutions using various splines when $\gamma = 0.9, \tau = 0.01, T = 1$ for Example 3

s	TuBS	CuBS	ECuBS	4 term solution [1]	Exact ($\gamma = 1$)
0.1	0.47299	0.47301	0.47331	0.48834	0.47385
0.2	0.46027	0.46032	0.46082	0.47662	0.46178
0.3	0.44775	0.44783	0.44842	0.46483	0.44969
0.4	0.43541	0.43541	0.43624	0.45299	0.43759
0.5	0.42326	0.42334	0.42411	0.44112	0.42551
0.6	0.41131	0.41132	0.41210	0.429221	0.41344
0.7	0.39956	0.39964	0.40035	0.41728	0.40141
0.8	0.38803	0.38803	0.38863	0.40535	0.38942
0.9	0.37672	0.37672	0.37702	0.39343	0.37751

Table 14: Comparison of approximate solutions using various splines when $\gamma = 0.75, \tau = 0.01, t = 1$ for Example 3

s	TuBS	CuBS	ECuBS	4 term solution [1]	Exact ($\gamma = 1$)
0.1	0.47198	0.47204	0.47252	0.50101	0.47385
0.2	0.45855	0.45863	0.45942	0.48941	0.46178
0.3	0.44557	0.44563	0.44684	0.47772	0.44969
0.4	0.43299	0.43304	0.43434	0.46595	0.43759
0.5	0.42080	0.42083	0.42224	0.45413	0.42551
0.6	0.40898	0.40994	0.41035	0.44225	0.41344
0.7	0.39754	0.39754	0.39873	0.43034	0.40141

(Continued)

Table 14 (continued)

s	TuBS	CuBS	ECuBS	4 term solution [1]	Exact ($\gamma = 1$)
0.8	0.38649	0.38653	0.38744	0.41841	0.3894
0.9	0.37585	0.37583	0.37645	0.40645	0.37757

Table 15: Comparison of approximate solutions using various splines when $\gamma = 0.5, \tau = 0.01, t = 1$ for Example 3

s	TuBS	CuBS	ECuBS	4 term solution [1]	Exact ($\gamma = 1$)
0.1	0.472332	0.47234	0.47283	0.51163	0.47385
0.2	0.459201	0.45924	0.45993	0.50013	0.46182
0.3	0.446445	0.44645	0.44744	0.48853	0.44969
0.4	0.434023	0.43403	0.43502	0.47685	0.43759
0.5	0.421907	0.42194	0.42294	0.46509	0.42551
0.6	0.410078	0.41014	0.41103	0.45325	0.41344
0.7	0.398531	0.39853	0.39944	0.44137	0.40141
0.8	0.387268	0.38732	0.38793	0.42944	0.38942
0.9	0.376304	0.37632	0.37674	0.41747	0.37751

Table 16: Comparison of absolute error using trignometric B spline with absolute error of first three terms solutions when $\gamma = 0.9, \tau = 0.01, t = 1$ for Example 3

s	TuBS	4 term solution [1]	Exact when $\gamma = 1$	Absolute error [1]	Absolute error TuBS
0.1	0.47299	0.48834	0.47385	0.01499	0.00086
0.2	0.46027	0.47662	0.46178	0.01484	0.00151
0.3	0.44775	0.46483	0.44969	0.01514	0.00194
0.4	0.43541	0.45299	0.43759	0.01540	0.00218
0.5	0.42326	0.44112	0.42551	0.01561	0.00225
0.6	0.41131	0.429221	0.41344	0.015781	0.00213
0.7	0.39956	0.41728	0.40141	0.01587	0.00185
0.8	0.38803	0.40535	0.38942	0.01593	0.00139
0.9	0.37672	0.39343	0.37751	0.01592	0.00079

Table 17: Spatial convergence corresponding L_∞ error at different values of M for Example 3 at time $t = 1$, $\tau = \frac{1}{100}$ and $\gamma = 0.9$

M	L_∞ Error	p_h
10	3.63933×10^{-3}	————
20	3.61059×10^{-3}	2.00503
40	3.60343×10^{-3}	2.0000
80	3.60164×10^{-3}	1.99160
160	3.60119×10^{-3}	—————

Table 18: Temporal convergence corresponding L_∞ error at different values of τ for Example 3 at time $t = 1$, $M = 20$ and $\gamma = 0.9$

τ	L_∞ Error	$p_{\Delta t}$
$\frac{1}{10}$	1.16757×10^{-2}	————
$\frac{1}{20}$	2.91255×10^{-3}	2.02900
$\frac{1}{40}$	7.66505×10^{-4}	1.93570
$\frac{1}{80}$	2.05566×10^{-4}	1.63420
$\frac{1}{160}$	2.48633×10^{-5}	—————

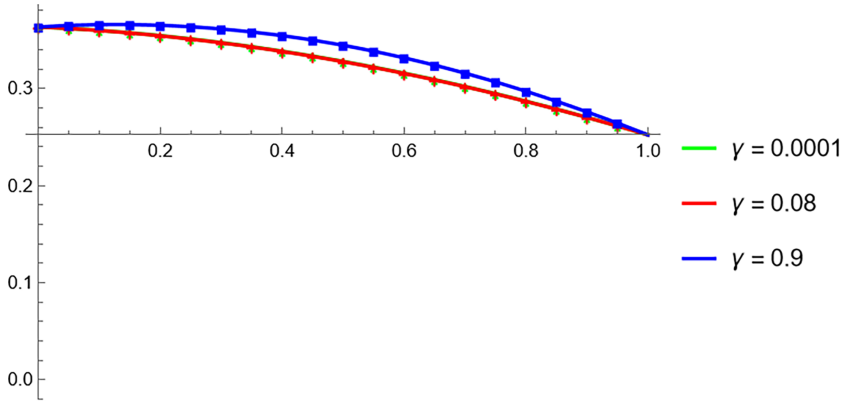

Figure 7: Comparison of approximate solutions at various γ using TCuBS when $h = \frac{1}{80}$, $\tau = 0.01$, $t = 1$

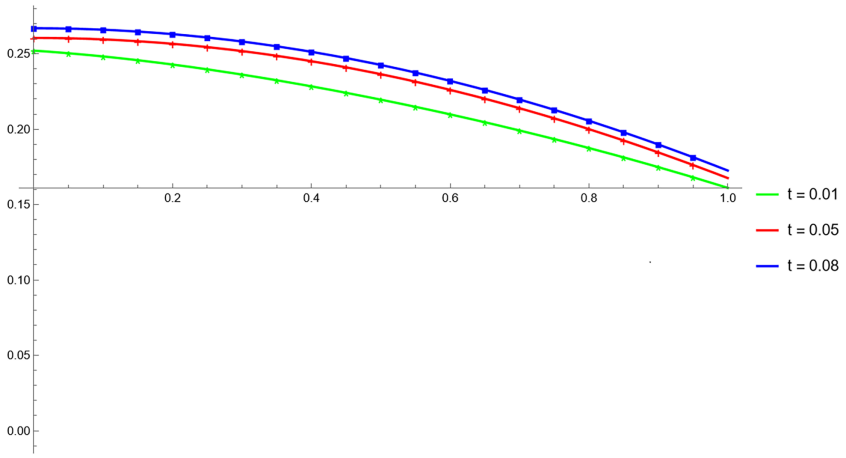

Figure 8: Comparison of the approximate solution at different values of t using TCuBS when $h = \frac{1}{80}, \tau = 0.01, \gamma = 0.8$

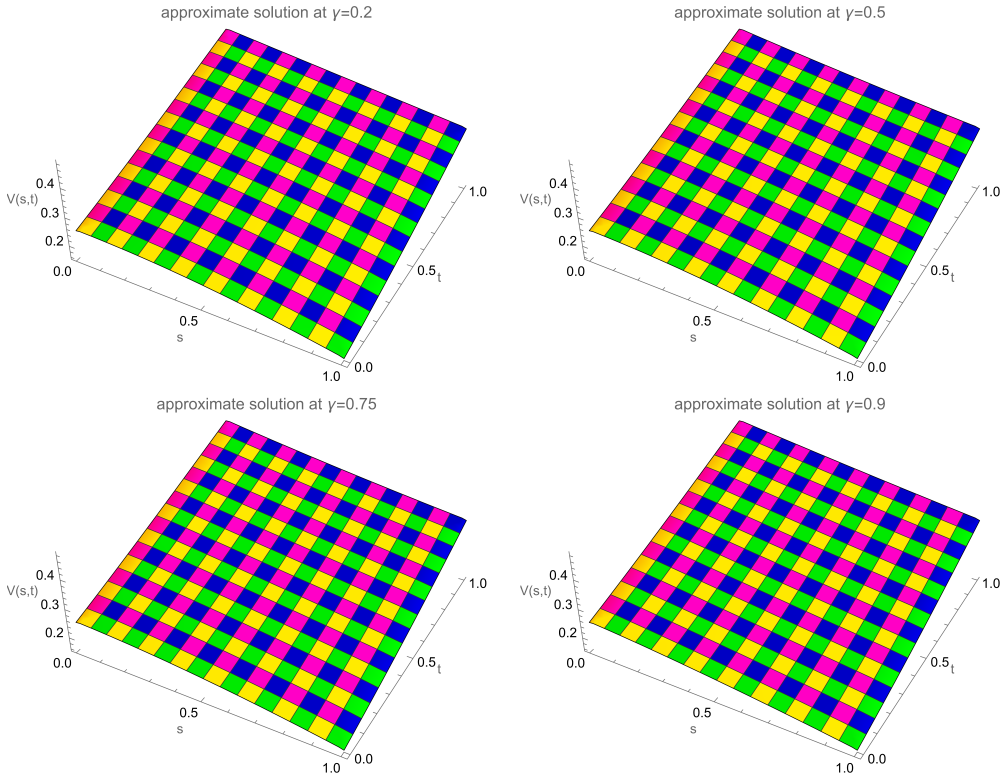

Figure 9: 3D approximate solutions for Example 3 at different γ using TCuBS when $h = \frac{1}{80}$, $\tau = 0.01$, and $t = 1$

6 Physical Interpretation of Numerical Results

The quantitative results shown in 2D Figures give physical insight into the dynamics of the time-fractional Newell-Whitehead-Segel equation. The 2D spatial plots are pattern amplitudes in population densities, chemical concentration waves, or neural activity, showing how initial disturbances develop. The 3D surface plots encode the complete spatiotemporal development, in which the fractional order γ has a direct control over memory effects and anomalous subdiffusion; $\gamma < 1$ accounts for transport across intricate media such as biological tissues or porous materials, resulting in a retardation of propagation and stabilization of patterns relative to regular diffusion ($\gamma = 1$). In addition, comparison over various values of γ brings out the transition from subdiffusive to normal transport, and plots of error identify numerical sensitivity regions usually corresponding to physical stability regions. Together, all these graphics illustrate how fractional derivatives with non-local kernels better describe pattern formation dynamics in systems that possess hereditary characteristics and spatial heterogeneity.

7 Concluding Remarks

This study has developed numerical solutions for the time-fractional Newell-Whitehead-Segel equation with a Caputo-Fabrizio derivative, employing three B-spline-based methods for spatial discretization: cubic, trigonometric cubic and extended cubic B-splines. Supported by rigorous stability and convergence analysis, the numerical results confirm the accuracy and robustness of all three schemes. Each method exhibits distinct strengths. Cubic B-splines offer a balance of simplicity and efficiency, making them suitable for general-purpose approximations. Trigonometric cubic B-splines demonstrate superior performance for problems with inherent oscillatory or periodic behavior. Extended cubic B-splines provide the highest degree of flexibility and accuracy, particulary for handling complex geometries or boundary conditions. The fractional order γ was shown to significantly influence the solution, underscoring the critical role of incorporating memory effects. The Caputo-Fabrizio derivative, with its non-singular kernel, proved effective in modeling these nonlocal temporal dynamics. Overall, the results highlight the potential of B-spline-based techniques as a powerful and versatile framework for solving time-fractional partial differential equations. Key advantages include exceptional numerical accuracy, computational efficiency via sparse systems and a firm theoretical foundation established through stability and convergence proofs. We acknowledge certain limitaions, including computational costs at high resolutions, the need for parameter tuning in the extended cubic B-spline formulations and validation constraints due to the limited availability of exact fractional-order solutions. Future work may focus on extending these methods to multi-dimensional and coupled systems, incorporating variable-order fractional derivatives and exploring adaptive mesh refinement to enhance accuracy. These limitations and extensions present valuable opportunities for future research.

Acknowledgement: We acknowledge the support of the Deanship of Scientific Research, Vice Presidency for Graduate Studies and Scientific Research, King Faisal University, Saudi Arabia.

Funding Statement: This work was supported by the Deanship of Scientific Research, Vice Presidency for Graduate Studies and Scientific Research, King Faisal University, Saudi Arabia (Grant No. KFU254494).

Author Contributions: Conceptualization, Muhammad Yaseeen and Marryam Shafique; methodology, Salma Trabelsi and Marryam Shafique; software, Muhammad Yaseeen; validation, Marryam Shafique

and Marwa Balti; formal analysis, Salma Trabelsi and Marwa Balti; investigation, Marryam Shafique, Muhammad Yaseeen and Salma Trabelsi; writing—original draft preparation, Marryam Shafique and Muhammad Yaseeen; data curation, Muhammad Yaseeen, Salma Trabelsi and Marwa Balti; visualization, Muhammad Yaseeen and Marwa Balti; funding acquisition, Salma Trabelsi, Marwa Balti. All authors reviewed and approved the final version of the manuscript.

Availability of Data and Materials: Not applicable.

Ethics Approval: Not applicable.

Conflicts of Interest: The authors declare no conflicts of interest.

References

1. Merdan M, Şahin Y, Açıkgöz P, Rashid A. The novel numerical solutions for Caputo-Fabrizio fractional Newell-Whitehead–Segel equation using Aboodh-ADM. PLoS One. 2024;9(1):e83265. doi:10.21203/rs.3.rs-4287125/v1.
2. Bokhari AH, Kara AH, Zaman FD. On the solution and conservation laws of the model for tumor growth in the brain. J Math Anal Appl. 2009;350(1):256–1. doi:10.1016/j.jmaa.2008.09.065.
3. Metzler R, Klafter J. The random walk's guide to anomalous diffusion: a fractional dynamics approach. Phys Rep. 2000;339(1):1–77. doi:10.1016/s0370-1573(00)00070-3.
4. Mainradi F. Fractals and fractional calculus in continuum mechanics. Berlin/Heidelberg, Germany: Springer-Verlag; 1997.
5. Diethelm K, Freed AD. On solution of nonlinear fractional order differential equations used in modelling of viscoplasticity. In: Scientific computing in chemical engineering II: computational fluid dynamics, reaction engineering and molecular properties. Berlin/Heidelberg, Germany: Springer-Verlag; 1999. p. 217–24. doi: 10.1007/978-3-642-60185-9_24.
6. Hilfer R. Applications of fractional calculus in physics. Singapore: World Scientific; 2000.
7. Sokolov IM, Klafter J, Blumen A. Fractional kinetics. Phys Today. 2000;55(11):48–54. doi:10.1063/1.1535007.
8. Sokolov IM, Blumen A. Ballistic vs. diffusive pair-dispersion in the Richardson regime. Phys Rev E. 2000;61(3):2717–22. doi:10.1103/physreve.61.2717.
9. Chen W. A speculative study of 2/3-order fractional Laplacian modeling of turbulence: some thoughts and conjectures. Chaos. 2006;16(2):1–6. doi:10.1063/1.2208452.
10. Korkmaz A. Complex wave solutions to mathematical biology models I: newell-Whitehead–Segel and Zeldovich equations. J Comput Nonlinear Dyn. 2018;13(8):7.
11. Kumar D, Sharma RP. Numerical approximation of Newell-Whitehead–Segel equation of fractional order. Nonlinear Eng. 2016;5(2):81–6. doi:10.1515/nleng-2015-0032.
12. Patel YF, Dhodiya JM, Pandit D. Exact solution of nonlinear Newell-Whitehead–Segel equation using semi-analytical approach. Math Methods Appl Sci. 2025;48(7):7149–65. doi:10.1002/mma.8843.
13. Kumar H, Yadav N. Approximate solution of Newell–Whitehead–Segel equation using deep learning method. In: Congress on intelligent systems. Singapore: Springer Nature; 2023. p. 405–14.
14. Bekela AS, Deresse AT. An efficient numerical method for nonlinear time fractional hyperbolic partial differential equations based on fractional Shehu transform iterative method. J Appl Math. 2025;2025(1):7007124.
15. Shawagfeh NT. Analytical approximate solutions for nonlinear fractional differential equations. Appl Math Comput. 2002;131(2–3):517–29. doi:10.1016/s0096-3003(01)00167-9.

16. Patade J, Bhalekar S. Approximate analytical solutions of Newell-Whitehead–Segel equation using a new iterative method. World J Model Simul. 2015;11(2):94–103. doi:10.21203/rs.3.rs-3231176/v1.
17. Saadeh R, Alaround M, Al-Samdi M. Application of fractional residual power series algorithm to solve Newell-Whitehead–Segel equation of fractional order. Symmetry. 2019;11(12):13.
18. Luo X, Nadeem M. Laplace residual power series method for the numerical solution of time-fractional Newell-Whitehead–Segel model. Int J Numer Methods Heat Fluid Flow. 2023;33(7):2377–91. doi:10.1108/hff-01-2023-0001.
19. Saravanan A, Magesh N. A comparison between the reduced differential transform method and the Adomian decomposition method for the Newell-Whitehead–Segel equation. J Egypt Math Soc. 2013;21(3):259–65. doi:10.1016/j.joems.2013.03.004.
20. Ayata M, Ozkan O. A new application of conformable Laplace decomposition method for fractional Newell-Whitehead–Segel equation. AIMS Math. 2020;5(6):7402–12. doi:10.3934/math.2020474.
21. Prakash A, Goyal M, Gupta S. Fractional variational iteration method for solving time-fractional Newell-Whitehead–Segel equation. Nonlinear Eng. 2019;8(1):164–71. doi:10.1515/nleng-2018-0001.
22. Areshi M, Khan A, Shah R, Nonlaopon K. Analytical investigation of fractional-order Newell-Whitehead–Segel equations via a novel transform. AIMS Math. 2022;7(4):6936–58. doi:10.3934/math.2022385.
23. Jassim HK. Homotopy perturbation algorithm using Laplace transform for Newell-Whitehead–Segel equation. Int J Adv Appl Math Mech. 2015;2(4):8–12.
24. Newell AC, Whitehead JA. Finite bandwidth, finite amplitude convection. J Fluid Mech. 1969;38(2):279–303. doi:10.1017/s0022112069000176.
25. Jani HP, Singh TR. Aboodh transform homotopy perturbation method for solving fractional-order Newell-Whitehead–Segel equation. Math Methods Appl Sci. 2022;47(15):12028–43. doi:10.1002/mma.8886.
26. Caputo M, Fabrizio M. A new definition of fractional derivative without singular kernel. Prog Fract Differ Appl. 2015;2(1):1–13. doi:10.18576/pfda/090405.
27. Caputo M, Fabrizio M. Applications of new time and spatial fractional derivatives with exponential kernels. Prog Fract Differ Appl. 2016;2(1):1–11. doi:10.18576/pfda/020101.
28. Venkateswaran J, Son YJ, Jones AT, Min HSJ. A hybrid simulation approach to planning in a VMI supply chain. Int J Simul Process Model. 2006;2(3–4):133–49. doi:10.1504/ijspm.2006.012642.
29. Yousif MA, Hamasalh FK. A hybrid non-polynomial spline method and conformable fractional continuity equation. Mathematics. 2023;11(17):3799. doi:10.3390/math11173799.
30. Abbas M, Majid AA, Ismail AIM, Rashid A. Application of cubic trigonometric B-spline to the numerical solution of hyperbolic problems. Appl Math Comput. 2014;239(3):74–88. doi:10.1016/j.amc.2014.04.031.
31. Sadeghi S. Computational approach for fractal mobile-immobile transport with Caputo-Fabrizio fractional derivative. Math Model Comput. 2022;12(4):249–63.
32. Liu Z, Cheng A, Li X. A second-order Crank-Nicolson scheme for fractional Cattaneo equation based on new fractional derivative. Appl Math Comput. 2017;311(4):361–74. doi:10.1016/j.amc.2017.05.032.
33. Siddiqi SS, Arshed S. Quintic B-spline for the numerical solution of the good Boussinesq equation. J Egypt Math Soc. 2014;22(2):209–13. doi:10.1016/j.joems.2013.06.015.
34. Abbas M, Majid AA, Ismail AIM, Rashid A. Numerical method using cubic B-spline for a strongly coupled reaction-diffusion system. PLoS One. 2014;9(1):e83265. doi:10.1371/journal.pone.0083265.
35. Manzoor MU, Yaseen M, Awadalla M, Zaway H. A uniform hyperbolic polynomial B-spline approach for solving the fractional diffusion-wave equations in the Caputo-Fabrizio sense. AIMS Math. 2025;10(7):17049–81. doi:10.3934/math.2025765.
36. Quarteroni A, Sacco R, Saleri F. Numerical Integration. In: Numerical mathematics. Berlin/Heidelberg, Germany: Numerical Mathematics; 2007. p. 379–422.